A mimetic numerical scheme for multi-fluid flows with thermodynamic and geometric compatibility on an arbitrarily moving grid

Thibaud Vazquez-Gonzalez, Antoine Llor, Christophe Fochesato

A mimetic numerical scheme for multi-fluid flows with thermodynamic and geometric compatibility on an arbitrarily moving grid

Thibaud Vazquez-Gonzalez, Antoine Llor*, Christophe Fochesato[1]

CEA, DAM, DIF, F-91297 Arpajon Cedex, France

Abstract

Simulating transient and compressible multi-fluid flows in extreme situations such as Inertial Confinement Fusion is especially challenging because of numerous and sometimes conflicting constraints: large number of fluids, both isentropic and strongly shocked compressible evolution, highly variable, stiff or contrasted equations of state, large heat sources, large deformations, and transport over large distances. Models and schemes for such flows all share a common non-dissipative "backbone" structure of per-fluid mass, momentum, and energy evolution-and-transport equations, coupled through pressure terms.

A novel and efficient multi-fluid numerical scheme for solving the backbone equations over a moving grid (ALE or Arbitrary Lagrangian–Eulerian) is here generated through a "Geometry, Energy, and Entropy Compatible" mimicking procedure [Eur. J. Mech. B – Fluids **67**, 494 (2017)]. Starting from the discretized density and energy fields, and transport operator, the procedure yields the discrete evolution equations in a practically univocal way. With arbitrarily moving grids, number of fluids, contrasts of volume fractions and equations of state, the resulting scheme is fully conservative in masses, momentum, and energy, preserves isentropic behavior to the scheme order, and ensures per-fluid thermodynamic consistency. Noticeably, optimal isentropic behavior is obtained thanks to a non-standard downwind form of pressure gradient.

Multi-fluid numerical test cases—including Sod's shock tube, Ransom's faucet, and a nine-fluids crossing test—are performed in two-dimensions using deliberately strenuous grid motion strategies. The results confirm the expected properties and illustrate the robustness, stability and versatility of the scheme at finite resolution, though it is not intended to be used as is. The scheme is a foundation block to be complemented with (system-dependent and ubiquitous) physical dissipation terms which provide the necessary damping of divergingly unstable modes at vanishing wavelengths.

Keywords: Multi-fluid flow, Arbitrary Lagrangian Eulerian, compatible scheme, thermodynamic consistency, shock, least action principle

1. Introduction

TO REVIEWERS: The introduction has been substantially improved in terms of length and legibility with splitting of new Section 2 and new Section 1.5. It now stresses the specific findings of this work that were questioned by Reviewer 1 and addresses the issues of conservation and convergence that were also questioned by Reviewer 2.

1.1. Motivations: multi-fluid flow simulation

In many areas of industry (combustion, nuclear, propulsion, health, pharmaceuticals, etc.) and academia (astrophysics, geophysics, meteorology, etc.) fluid flows may involve dispersed multiple phases (liquid, gas, solid, and their combinations) or components (individual particles, droplets, bubbles, etc.). Due to the high variety and complexity of interactions between mixed phases—with widely disparate scales of pressure gradients, flow speeds, material properties, etc.—accurate and fully detailed descriptions of such systems remain inaccessible except for simple or ideal cases depending on nature, strength, boundaries, sources, etc. However, there are numerous, complex, and important situations which have to be dealt with, even if in approximate ways, as for instance with bubbles and slugs in pipes [1–3], nuclear reactor safety [4–6], cavitation [7], dust combustion and explosions [8–10], fluidized beds [11], volcanic eruptions [12], atomization in combustion [8, 13, 14], deflagration and detonation [15, 16], hydro-cyclone separators [17–19], sloshing in tanks [20], etc.

A widely used approach to describe flows containing multiple components is the so-called multiphase or multi-fluid modeling based on a time, space, or ensemble *phase-conditional average* [see for instance 21–26, for details]. Phase-conditional averaging operators are applied directly to single-phase local-and-instantaneous mass, momentum, and energy equations and,

*Corresponding author
Email addresses: thibaud.vazquez-gonzalez@cea.fr (Thibaud Vazquez-Gonzalez), antoine.llor@cea.fr (Antoine Llor), christophe.fochesato@cea.fr (Christophe Fochesato)
[1]Present address: CEA, DEN, CAD, F-13108 Saint-Paul-lez-Durance Cedex, France

after closure of unknown correlations, a broad variety of models can be produced—depending on phase characteristics, dispersion geometry, flow regime, dissipation processes, source terms, boundary conditions, etc.

When stripped of all dissipation effects however, *all the multi-fluid models display a common structure* of coupled Euler-like fluid evolution equations for masses, momenta, and energies *involving transport and pressure terms only*. In the vast majority of systems, the fluid pressures also relax towards a common pressure field and the authors designate the ensuing set of equations as the "backbone model." For two fluids, this model is usually known as the "single-pressure six equation model" [27, 28, and references therein].[2] The backbone model plays a central role in the analysis of multi-fluid numerical schemes and will be the main object of the present work.[3]

Independently of model details, the numerical resolution of multi-fluid flow equations has remained challenging to this day due to various of their features which happen to be almost all retained in their associated backbone model equations: i) they cannot be expressed in fully conservative form because of pressure couplings [as noticed for instance in 32, § 2.3]; ii) they may involve stiff terms when fluid properties are strongly contrasted (for example with highly variable or different EOS characteristics) [as noticed for instance in 28, eq. 5 and comments]; iii) they may be partially elliptic for subsonic inter-fluid drift velocities—which produce divergingly fast unstable modes at vanishing wavelengths;—and last but foremost here iv) their thermodynamic consistency—compliance with the first and second laws of thermodynamics, the latter of which forbids entropy reduction in a closed system and ensures entropy preservation for vanishing dissipation,—can be lost in many numerical integration schemes involving inconsistent calculations of pressure work.

1.2. Ellipticity: a major and widely explored issue in multi-fluid simulations

Ellipticity of the backbone system (point iii above in Section 1.1) has been recognized as an important and recurring issue as reviewed for instance in Ref. [33]. The model displays unstable behavior with discontinuous dependence with respect to initial conditions: it is thus ill-posed in the sense of Hadamard. Therefore, although the backbone model can be discretized in many consistent ways, the ensuing discrete models cannot be made to converge for vanishing cell size on any test case.

However, the backbone model is not intended to be used as is but complemented with other physical dissipation processes. These are system-dependent but ubiquitous and *always* involve a cutoff length scale (for instance the size of particles or droplets, the width of a duct, etc.) around which some efficient dispersion and dissipation effects exist—and below which the continuous multi-fluid description does not make much sense anyway. Therefore if the system displays instabilities, these are confined to length scales larger than the cutoff where the growth rate is bounded by the growth rate of the backbone model at cutoff. As already noticed by numerous investigators [32–40] continuity with respect to initial conditions is then recovered. A more elaborated and formal discussion is provided in Appendix A with quotes from the aforementioned references.

Now, *at fixed finite resolution*, discretized backbone models experience a cutoff scale given by cell size where numerical dissipation damps instabilities just as a physical dissipation process would do. It is thus possible to carry out calculations, limited in time and resolution, with discretized backbone models. In this spirit, *the numerical examples provided in the present work do not test convergence but* robustness *and* consistency *at* fixed finite resolution. *The present numerical scheme is merely a* foundation block *to be complemented with system-dependent dissipation terms which provide the necessary damping to eventually reach convergence.*[4]

1.3. Thermodynamic consistency: another major but less explored issue in multi-fluid simulations

In contrast to ellipticity, thermodynamic consistency (point iv above in Section 1.1) has drawn much less attention, leaving many elements to be clarified, but more or less implicitly it has been looming over and been coped with in the development of most multi-fluid models [41] and hydro-schemes. For instance, it was pointed out [28] that entropy errors in calculations may come from numerical residues on i) cell volume variations, ii) relative-to-grid transport, and iii) volume fraction coupling between drifting fluids, especially when solving with respect to an arbitrarily moving grid. Analysis of these errors requires disentangling all the contributions and is thus seldom performed.[5] Now, being produced by the discretization of the pressure terms, the entropy errors are identical in both backbone and full "fleshed up" versions of the models: the backbone model here appears as the critical benchmark for thermodynamic consistency. At this point, it must be stressed that this

[2] Usage of word "model" for the set of backbone equations can be misleading but is now ingrained by over fifty years of custom: very few physical situations can actually be described by this idealized set of equations. Yet, among these, two cases of practical impact must be noticed: *separated flows* whose instabilities are critical for pipe slugging [see for instance 1, and references therein], and *numerical interfaces* in mixed cells which formally follow the very same equations [see for instance 29–31, and references therein].

[3] It is worth reminding that the extremely high rates of physical pressure oscillations and relaxation processes in most systems justify the neglect of pressure differences when disregarding contributions from surface tension and added mass, but nevertheless, backbone-like models involving pressure imbalance closed by *algebraic* relationships still behave very similarly to the single pressure backbone model.

[4] As an extreme example, a numerical scheme to solve some given well-posed multi-fluid model could follow a splitting strategy whereby each time step would involve two successive evolution phases under the discretized equations of i) the backbone model and ii) the remaining pure dissipation processes. Although the backbone step could be viewed as unacceptable for its consistency with an ill-posed problem, the full scheme would be perfectly acceptable and converge towards the well-posed solution of the full model. Therefore, the scheme for the backbone model only provides a consistent discretization of the corresponding *operators* in the full model.

[5] The magnitude of this task can be illustrated by the example of a fully compressible dispersed flow described by a 12-section reduction of the particle distribution function (for instance over velocities, sizes, temperatures, etc.): this low but realistic number of sections leads to 13 separate isentropic conditions to hold when dissipation processes vanish, with $26 \times 25/2 = 325$ pressure-driven exchange terms between the 26 different kinetic and internal energy reservoirs.

consistency can be analyzed, both physically and numerically, *only by making the system perfectly non-dissipative and thus elliptic*: ellipticity thus becomes a *requirement* and not a nuisance.

A related and disturbing novel finding was reported in a previous publication by the authors [42, 43, § 2.6]: if a scheme preserves entropy to its order of accuracy on *isentropic* single-fluid flows, thermodynamic consistency *demands* that, if mass transport relative to the grid is *upwinded*, then pressure gradient in the momentum equation be *downwinded*. This immediately raises the issue of the pressure gradient discretization in multi-fluid schemes where fluids may be transported in opposite directions relative to the grid while being locally at same pressure: it is one of the major challenges that the present work will tackle.

It cannot be stressed enough that thermodynamic consistency has a strong impact on the simulation of multi-fluid systems: as recently reported by R.W. Lyczkowski [44, § 7.5 pp. 99–100 and § 7.6 pp. 110–111 on "Standard Problem 1"], the development of one of the earliest and major industrial codes for safety assessment of nuclear reactors was stalled for about two years to 1975 by what happened to be an inconsistent evolution of the underlying entropy. From the authors' experience, similarly extreme situations are not uncommon, even nowadays, though they may go unnoticed: many multi-fluid simulations appear misleadingly robust thanks to sufficiently large physical or numerical dissipation, or to quasi-incompressible behavior of all but one fluid. Yet, like a sword of Damocles, the fragility is hidden but present and can unexpectedly crash calculations when for instance changing numerical conditions, force closures, equations of state, etc.

1.4. Aim: compressible multi-fluid ALE numerical scheme

In the present work, a novel discretization of the backbone equations—to be included in numerical schemes for the simulation of strenuous multi-fluid flows as found in Inertial Confinement Fusion—is built in order to meet the following demands: i) large number of compressible fluids (only restricted by computing resources, for instance up to a few dozens) in order to eventually implement sectional approaches to particle distribution functions [45–48] (multi-size, but possibly multi-velocity, multi-temperature, etc.); ii) both isentropic or strongly shocked fluid evolution; iii) for simplicity, no added mass nor surface tension effects (which in principle can be consistently added to the scheme); iv) highly variable and contrasted EOS stiffness (such as water and air for which acoustic impedance differs by a factor of 4000); and v) large deformations and advection over possibly large distances.

This list of constraints translates into the following fundamental algebraic properties of the numerical scheme: i) exact conservation of masses, momentum, and total energy up to round-off errors in order to ensure the proper capture of jump conditions in shocks; ii) thermodynamic consistency of pressure work to second-order regardless of mesh motions; iii) arbitrarily evolving computational mesh where grid motions can be either defined by the user beforehand or adjusted on-the-fly to the flow.

The last feature above is designated by ALE (Arbitrary Lagrangian–Eulerian) as first introduced for single-fluid flow [49, 50]: it allows to retain the advantages of both Eulerian and Lagrangian approaches which use meshes that respectively stay fixed or follow the fluid motion. Numerous ALE strategies have been designed for multi-material [51–55, and references therein] and multi-fluid applications [56, § 13], [57, and references therein]. In most of these works however, thermodynamic consistency appears to have been a relatively minor concern, possibly because they deal with practical situations where *all fluids except one* can be assumed to be weakly compressible (condensed phases) compared to the last one (gas).

Two broad categories of ALE strategies exist [42, 43, and references therein]: *indirect* and *direct*. Indirect ALE approaches perform a separation between Lagrangian evolution steps and a remapping procedure after arbitrary time increments. In contrast, no remap step is used in direct ALE as mass, momentum and energy fluxes at moving cell boundaries are directly taken into account in the discrete evolution equations. Indirect ALE approaches have been used for multi-fluid multi-velocity flows [58]: as a major advantage, they can ensure thermodynamic consistency upfront because the Lagrangian evolution is intrinsically consistent and remap is dissipative, but they become computationally expensive for multi-fluid systems in two- or three-dimensions due to remapping [59]. In contrast, direct ALE approaches appear more computationally efficient as they do not involve remap steps but they can be challenged by the capture of the pressure work in a thermodynamically consistent way. Relaxing the thermodynamic consistency constraints could be achieved by using multiple superposed meshes for the different fluids, as was shown for 1D two-fluid slug flows with a more complex double ALE strategy [60, 61]. The present work will be devoted to a *common-mesh direct ALE* scheme for multi-fluid flows.

1.5. General relevance of the present numerical scheme

TO REVIEWERS: New section, see note to reviewers in Introduction.

Many of the demands that the numerical scheme must meet (points i) to v) in Section 1.4) have been explored in (sometimes numerous) previous publications, but mostly *separately*: integrating all these constraints simultaneously does not seem to have ever been attempted. In course of the present work, ensuring compressible-yet-consistent (isentropic) thermodynamics on multi-fluid flows over a fully arbitrary ALE grid appeared as a major challenge that eventually required developing a novel and original discretization approach, here designated as "GEEC" for "Geometry, Energy, and Entropy Compatible." The GEEC approach hinges on an very general *variational* construction whose fundamental premises are exposed in Section 2 before being applied to the present multi-fluid scheme in Sections 3 and 4.

The present scheme may look somewhat limited by some of its features, in particular for its order one transport with respect to the grid. However, rigorous thermodynamic consistency already makes it valuable in "real" applications especially when numerical diffusion is not dominant. But even beyond that, it

must be considered foremost as a successful *proof of concept* which, within the GEEC framework, opens the possibility of numerous extensions—both numerical (higher orders, boundary conditions, three dimensions, etc.) and physical (viscosity, collisions, etc.)—but further, provides new perspectives to multi-fluid numerical schemes in general.

This specific status of the scheme appears in the somewhat unusual structure of the present document. The derivation is discussed at length as most of the concepts involved are foreign to the dominant finite volumes and finite elements communities. Some of scheme's features are established in a rigorous formal way (such as consistency; exact conservation laws; entropic character to the scheme order; arbitrary mesh structure, dimension, or ALE capability; etc.) and are not tested on reported "numerical experiments"—but have of course been checked in the course of code developments [42]. To preserve legibility, reported benchmarks are kept to just a few, but more of them have been carried out [42]. The tests have been selected for their widespread usage and accepted relevance in hydro-schemes, with a last one specifically tailored to highlight all the scheme's features together on a short animated representation. Also noticeable is that, except for the classical Ransom faucet test, the benchmark cases are in fact "superficially classical:" they involve the physical flows of classical tests but are computed under much more scheme-strenuous numerical conditions. Convergence tests have been carried out but are not reported as the interfering ellipticity issues are out of the scope of the present work (see Section 1.2) and emphasis is here on robustness and consistency.

1.6. General structure of the present work

The variational direct ALE scheme is thus derived according to the GEEC principles discussed in Section 2. Because the discretized equations are obtained by mimicking the derivation of the continuous evolution equations from first principles, the presentation is structured in two main parts: i) Section 3 provides the continuous guideline where coupled evolution equations for each fluid's momentum and internal energy are obtained from the least action principle and Gibbs relationship; and ii) Section 4 provides the derivation of the coupled increment equations for fluids' mass, momentum and internal energy which mimic the continuous equations of Section 3. The sections are split into mirroring subsections as detailed in Table 1 and grouped in the three geometry, energy, and entropy steps of the GEEC approach presented in Section 2.3

Readers who may not be interested in the step-by-step derivation of the increment equations of the scheme can skip Sections 2 to 4, and go to Section 5 where a summary of the multi-fluid algorithm is presented, along with the time step definition and the near-Lagrangian velocity reconstruction. Notations are given in Appendix B.

When reduced to one fluid, the final scheme mostly coincides to second order with the previous GEEC single-fluid scheme developed by the authors [42, 43]: here, because of the complexity of inter-fluid pressure couplings, the discrete internal energy equations have not been fully corrected for second-order-in-time entropy errors.

Results of tests in Section 6—variants of Sod's shock tube, Ransom's water faucet, and the crossing of eight Gaussian clouds of heavy fluids in a surrounding light gas—illustrate the different built-in properties of the scheme in terms of geometric, energetic, and entropic compatibility. Other test results were reported previously [42, § 4.5] and an animation of the eight Gaussian clouds crossing test is available as supporting information on the journal website.

2. Basic principles for the present "GEEC" discretization approach

TO REVIEWERS: New section, see note to reviewers in Introduction.

2.1. Mimetic discrete variational derivation

Among the specifications of the numerical scheme listed in Section 1.4, the proper isentropic behavior appears as an especially *fragile* but *central* property. It is fragile because, in principle, even the slightest errors on internal energy integration—for instance of numerical origin—are physically forbidden if of wrong sign: they can crash calculations by uncontrolled run offs of thermodynamic quantities. Though a successful isentropic calculation may appear quite uneventful, especially if returning to its initial state, it is nevertheless no simple task as it is "living at the edge of stability" as quoted from Ascher and McLachlan [66, § I]. This was exemplified in a short overview of published results on Ransom's faucet test case [28], which is essentially an isentropic flow. Now, despite this fragility, isentropic behavior is central because it is *unique*, and if numerically tractable, it ensures that *all* the possible dissipative behaviors of the system also become accessible: dissipation processes are merely added to the equations, the proper sign of entropy production terms being simply ensured by elementary algebraic relationships.

This strategy of first building an isentropic solver[6] is in contrast with that of many common numerical schemes, mostly derived from Godunov's scheme [68] and relying on Riemann solvers, which are intrinsically dissipative and may become difficult to adapt in convoluted systems [67]: in this respect, multi-fluid systems are emblematic as the conservation equations do not yield unique (Hugoniot) jump relationships as for single-fluid shocks. Next to an infinite number of acceptable dissipative evolution paths, there is only one isentropic evolution. As a related consequence, the non-conservative parts of the pressure-coupling terms in the multi-fluid equations cannot be freely discretized and must match all the other discretized pressure terms in order to ensure isentropic behavior (up to the scheme order).

Previous investigations in single-fluid cases, in Lagrangian [64] and then direct ALE settings [42, 43], revealed a general principle that will be applied here to optimize the

[6] The first-ever designed Lagrangian hydro-scheme of von Neumann and Richtmyer [62] actually follows this "isentropy first, dissipation next" approach as reexamined in [64] and discussed more generally in [67].

GEEC step	"To mimic" subsections	Discretization subsections	Content	Comments, findings
I	3.1	4.1–4.2	Fields, mass transport, and action integral definitions	Ensure simple second-order geometric consistency and preserve legacy with previous space- and time-staggered Lagrangian schemes [62–65]
I	3.2	4.3	Euler–Lagrange equations	
I	3.3	4.4–4.5	Momentum equations	Involve specific discrete pressure gradients and adapted transport operators
II	3.4	4.6	Kinetic energy equations	Required to build internal energy equations in next step
II	3.5	4.7	Internal energy equations	Explicit, ensure total energy conservation
III	3.7	4.8	Artificial viscosity	Required for shock capture, only added dissipation process in present work
		4.9	Discrete pressure closure	Supplementary (non-mimicked) step for exact equal fluid pressures

Table 1: Structure of the scheme derivation in the present work showing correspondence between the GEEC steps designated as I, II, and III (for respectively Geometry, Energy, and Entropy), the continuous derivation to be mimicked in Subsections 3, and the discrete derivation in Subsections 4.

multi-fluid numerical scheme with respect to isentropic behavior: *isentropic flow is geometric* [67]. This summarizes the following chain of properties: i) internal energies under isentropic conditions depend only on *volumes*, which in turn depend only on the *positions* of the fluid elements; ii) the total internal energy is thus a *potential* whose gradient produces all the non-dissipative forces in the system; iii) the system can thus be described by a *Lagrangian functional* within the general framework of the *least action principle*; and iv) corresponding quasi-isentropic numerical schemes can be obtained from a mimetic approach, by *minimizing discretized action integrals* [69]. This is just a special case of more general geometric mimicking principles reviewed in Refs [66, § I], [70], and [71, § I], to which a special issue of the *J. Comput. Phys.* was recently devoted [72]. Effective hydrodynamic schemes are eventually produced by correcting possible numerical residues to recover conservation properties and by adding physical dissipation terms—especially for shock stability. As in Ref. [43] this general course to generate schemes will be designated here by GEEC for "Geometry, Energy, and Entropy Compatible."

2.2. Least action principle in continuous fluid dynamics

The least action principle is a fundamental ingredient of mathematical physics and provides a unified theoretical framework to derive geometrically and energetically consistent equations of motion for a wide range of physical systems, from the simple harmonic oscillator to convoluted quantum gauge-field theories [73]. It can also be applied to fluid dynamics and its numerical schemes, as exemplified for the single-fluid ALE setting in a previous publication by the authors [42, 43]. The present work can thus be considered as a multi-fluid extension of this investigation and, although a short summary of the method is provided below, readers are strongly encouraged to become familiar with the basics of the voluminous background in the field and the technicalities of the scheme design respectively summarized and exposed in Ref. [43, §§ 1.2 & 2].

Though it is not a strict requirement for the design of GEEC discrete equations, mimicking the derivation of the continuous equations turns out to provide invaluable guidance to ensure the first step of "Geometric Compatibility:" once a continuous action integral is defined, the discretization is merely reduced to building an approximate quadrature for this integral whose discrete minimization yields the scheme's evolution equations. The procedure has been extensively studied on physical systems with finite degrees of freedom [69].

For single-fluid hydrodynamics—described by the Euler equation—two equivalent variational routes can be followed depending on the choice of the system's coordinates: Lagrangian or Eulerian. Readers interested in the intricacies of their progressive inception and development are referred for instance to Ref. [74, § I and references therein]. For the present study, it suffices to be retained that both approaches are now well understood but differ quite substantially in terms of Lagrangian definition and algebraic complexity of the action integral minimization. As expected, both Lagrangian [75] and Eulerian [76–78] derivations have been successfully adapted to two-fluid flows and can be readily extended to any number of fluids. However, for mimicking purposes in an ALE context with transport relative to the grid, the Eulerian setting will be privileged here as it involves a formally equivalent transport relative to the reference frame [42, 43].

2.3. Some general principles of the GEEC approach

Outside of the so-called SPH (meshless) methods [79, 80], applications of mimetic least action approaches to fluid dynamics schemes have been rather recent and scarce. Most relevant for the present study are 2D Eulerian [81] and ALE [82] viscous compressible flows, 1D Lagrangian [83] and ALE [84, 85] reacting thermo-compressible flows, ALE 1D Burgers equation [86], Eulerian rotating stratified flows [87], Eulerian incompressible flows [88], Eulerian rotating or shallow water flows [89], and ALE single-fluid compressible flows [42, 43]. A common feature in these works is the more or less explicit and accurate discretization of mass-transport constraints in the Lagrangian—as well as the possibly associated constraints on entropy and particle labeling fields—which critically affects the

order and the *holonomic* or *symplectic* character of the final schemes.

In most of these cases, transport is discretized by simple *first order* upwind fluxes which keep the derivation of the scheme tractable by hand but also make the *holonomy* approximate—though exact holonomy could be recovered in some schemes by integrating the configuration variables [88, 89]. In any case however, exact conservation of holonomy, momentum, and energy cannot be simultaneously preserved in a numerical scheme [69, 90]. Thus in the present study, momentum and energy will be exactly conserved and an approximately holonomic transport of each fluid will be discretized by upwind first-order cell-centered mass fluxes—very similar to those introduced in Refs [88, 89] and adopted in the previous single-fluid scheme [42, 43, §§ 2.2.1 eqs 12 & 14]. From there, second-order upgrading could appear as possible even if tedious to derive, but all known second-order flux formulas are actually incompatible with holonomy (even approximate) because of their non-linear (quadratic) dependence on velocity. The discrete Lagrangian functional, built from the discrete integrals of kinetic and internal energies and the discrete mass transport equations, fully defines the first "Geometric Compatibility" step of the GEEC approach.

The second "Energetic Compatibility" step of the GEEC approach aims at producing internal energy equations with thermodynamic consistency. In the single-fluid case, this is directly obtained through exact energy conservation: the energy tally with the discrete kinetic energy equation yields only one possible equation of internal energy. In the multi-fluid case however, this tally is not sufficient as internal energy transfers between fluids are possible and compatible with total energy conservation. It will thus be necessary to introduce supplementary constraints, namely the discretized fundamental thermodynamic relations on each fluid, which must preserve isentropic evolution to the scheme order. These must be carefully implemented as the explicit forms of the thermodynamic relations coupled by a common pressure exhibit various contributions of potentially highly contrasted stiffness [28, eqs 4 & 5].

The third "Entropic Compatibility" step consists in adding the irreversible energy processes through "dissipation potentials" as introduced by Lord Rayleigh [91, § II]. These entropy producing terms are here restricted to a multi-fluid artificial viscosity for shock capture, consistent with prescriptions by D.L. Youngs [25, § 8.3].

3. "To-mimic" variational derivation of multi-fluid hydrodynamics

3.1. Fields, action integral, and transport

As mentioned in Section 2.2, a derivation of the continuous multi-fluid Euler equations in Eulerian coordinates is provided here from the least action principle. It extends the two-fluid derivation of J.A. Geurst [76–78] to an arbitrary number of fluids Φ—labeled φ with $1 \leq \varphi \leq \Phi$,—with an explicit volume-filling constraint [75] and per-fluid Lin constraints as discussed in Refs [92, § 15 eq. 15.6], [93, § I.1 eq. I.1.6], and [94, eq. 15]. The Lin constraints represent in an Eulerian description the fact that all fluid elements can be ascribed a Lagrangian labeling coordinate: this ensures complete equivalence with Lagrangian descriptions. They appear here as a mere technicality and their variants and subtle connections to vorticity and entropy transport—already discussed at length elsewhere [92–96]—are beyond the scope of the present work.

The action integral is

$$\mathcal{A} = \iint \mathcal{L}(t,\boldsymbol{x})\,\mathrm{d}^3\boldsymbol{x}\,\mathrm{d}\,t\,, \tag{1}$$

where the Lagrangian density for the system of Φ fluids is

$$\begin{aligned}\mathcal{L} = \textstyle\sum_\varphi \Big(&\tfrac{1}{2}[\alpha\rho]^\varphi u_i^\varphi u_i^\varphi - [\alpha\rho]^\varphi e^\varphi(\rho^\varphi, s^\varphi(\xi^\varphi)) \\ &+ \phi^\varphi\,\mathrm{D}_t^\varphi[\alpha\rho]^\varphi + \psi^\varphi\,\mathrm{D}_t^\varphi[\alpha\rho\xi]^\varphi\Big) - \Pi\Big(\textstyle\sum_\varphi \alpha^\varphi - 1\Big)\,,\end{aligned} \tag{2}$$

and where $\alpha^\varphi(t,\boldsymbol{x})$, $\rho^\varphi(t,\boldsymbol{x})$, $\boldsymbol{u}^\varphi(t,\boldsymbol{x})$, and $\xi^\varphi(t,\boldsymbol{x})$ are respectively the fields of volume fraction, density, Eulerian velocity, and Lagrangian coordinate of fluid φ—$[\alpha\rho]^\varphi$ and $[\alpha\rho\xi]^\varphi$ standing respectively for $\alpha^\varphi\rho^\varphi$ and $\alpha^\varphi\rho^\varphi\xi^\varphi$. The internal energy e^φ is here taken to be a function of ρ^φ and entropy s^φ, the latter being a Lagrangian invariant field, i.e. a function of the Lagrangian coordinate ξ^φ: this defines an isentropic evolution for each fluid element but not necessarily with uniform entropy fields. D_t^φ and d_t^φ are respectively the so-called Eulerian and Lagrangian derivatives along fluid velocities $\boldsymbol{u}^\varphi$, as defined and connected through an extended product rule on any generic fields a and b

$$\mathrm{D}_t^\varphi\, a = \partial_t a + (u_i^\varphi a)_{,i}\,, \tag{3a}$$
$$\mathrm{d}_t^\varphi\, a = \partial_t a + u_i^\varphi a_{,i}\,, \tag{3b}$$
$$\mathrm{D}_t^\varphi(ab) = a\,\mathrm{D}_t^\varphi\, b + b\,\mathrm{d}_t^\varphi\, a = a\,\mathrm{d}_t^\varphi\, b + b\,\mathrm{D}_t^\varphi\, a\,. \tag{3c}$$

Einstein's notation of implicit summation on repeated coordinate indices is assumed—thus $\boldsymbol{\nabla}\cdot\boldsymbol{a} = a_{i,i}$ and $\boldsymbol{\nabla} b = b_{,i}\hat{\boldsymbol{e}}_i$. Lagrangian derivatives express evolution of material elements whereas Eulerian derivatives express evolution over fixed volume elements. The product rule is a key ingredient for variational derivations and conservation conditions which must thus be properly mimicked by the many possible discrete versions of the Eulerian and Lagrangian derivatives. Using the mass conservation condition one has

$$\mathrm{D}_t^\varphi[\alpha\rho\xi]^\varphi = [\alpha\rho]^\varphi\,\mathrm{d}_t^\varphi\,\xi^\varphi + \xi^\varphi\,\mathrm{D}_t^\varphi[\alpha\rho]^\varphi = [\alpha\rho]^\varphi\,\mathrm{d}_t^\varphi\,\xi^\varphi\,, \tag{4}$$

and thus the *conservation* equations for Lagrangian coordinates ξ^φ embedded in (2) are equivalent to their *invariance* along fluid trajectories. Usage of Eulerian instead of Lagrangian derivatives for expressing conservation constraints in (2) will be justified in Section 4.1.

The Lagrangian density (2) thus involves: i) the usual terms of per-fluid kinetic and potential (internal) energies, ii) the mass conservation constraints with multiplier fields $\phi^\varphi(t,\boldsymbol{x})$ which relate velocity and density fields, iii) the Lin constraints on Lagrangian coordinates with multiplier fields $\psi^\varphi(t,\boldsymbol{x})$, and iv) the volume-filling constraint with multiplier field $\Pi(t,\boldsymbol{x})$.

3.2. Euler–Lagrange equations, single pressure condition

The action integral minimization is performed over variations of the independent fields ϕ^φ, ψ^φ, ξ^φ, $[\alpha\rho]^\varphi$, $\boldsymbol{u}^\varphi$, ρ^φ, and Π. This of course could be carried out over any other combination of the fields but the present choice appears to be most convenient to simplify later calculations. α^φ must thus be substituted by $[\alpha\rho]^\varphi/\rho^\varphi$ in the volume-filling constraint of the Lagrangian expression (2). The action variation is thus

$$\begin{aligned}\delta\mathcal{A} = \iint \Big[\sum_\varphi \Big(&\frac{\partial\mathcal{L}}{\partial\phi^\varphi}\,\delta\phi^\varphi + \frac{\partial\mathcal{L}}{\partial\psi^\varphi}\,\delta\psi^\varphi + \frac{\partial\mathcal{L}}{\partial\xi^\varphi}\,\delta\xi^\varphi \\ &+ \frac{\partial\mathcal{L}}{\partial[\alpha\rho]^\varphi}\,\delta[\alpha\rho]^\varphi + \frac{\partial\mathcal{L}}{\partial u_i^\varphi}\,\delta u_i^\varphi + \frac{\partial\mathcal{L}}{\partial\rho^\varphi}\,\delta\rho^\varphi \Big) \\ &+ \frac{\partial\mathcal{L}}{\partial\Pi}\,\delta\Pi \Big] \mathrm{d}^3\boldsymbol{x}\,\mathrm{d}t\,, \end{aligned} \tag{5}$$

where the field variations are assumed independent, continuously differentiable, and vanishing at domain boundaries in t and $\boldsymbol{x}$. Partial derivatives with respect to each of the fields in (5) implicitly assume that the other fields are kept constant. Imposing $\delta\mathcal{A} = 0$ from extremal action (least action principle), performing integration by parts in (5) according to (3c), and dropping common factors yields the per-fluid Euler–Lagrange equations

$$0 = \mathrm{D}_t^\varphi [\alpha\rho]^\varphi\,, \tag{6a}$$
$$0 = \mathrm{D}_t^\varphi [\alpha\rho\xi]^\varphi\,, \tag{6b}$$
$$0 = T^\varphi \tfrac{\partial s^\varphi}{\partial\xi^\varphi} + \mathrm{d}_t^\varphi\,\psi^\varphi\,, \tag{6c}$$
$$0 = -\tfrac{1}{2}u_j^\varphi u_j^\varphi + e^\varphi + \Pi/\rho^\varphi + \mathrm{d}_t^\varphi\,\phi^\varphi + \xi^\varphi\,\mathrm{d}_t^\varphi\,\psi^\varphi\,, \tag{6d}$$
$$u_i^\varphi = \phi_{,i}^\varphi + \xi^\varphi\psi_{,i}^\varphi\,, \tag{6e}$$
$$\Pi = P^\varphi\,, \tag{6f}$$
$$1 = \textstyle\sum_\varphi \alpha^\varphi\,, \tag{6g}$$

where $P^\varphi = (\rho^\varphi)^2\partial e^\varphi/\partial\rho^\varphi$ and $T^\varphi = \partial e^\varphi/\partial s^\varphi$ are respectively the pressure and temperature fields of fluid φ.

The per-fluid Euler–Lagrange equations (6) display the following features: i) (6a) and (6b) represent respectively the per-fluid mass and Lagrangian-coordinate conservation equations; ii) (6c) represents the evolution equations of the Lagrange multipliers of Lin's constraints; iii) (6d) provides evolution equations of the system through the Lagrange multipliers ϕ^φ; iv) (6e) provides Clebsch decomposition of velocities as functions of Lagrange multipliers and shows that Lin's constraints $\psi_{,i}^\varphi \neq 0$ lift the irrotational restrictions; v) (6f) prescribes that *all fluids share a common pressure field* $P = \Pi = P^\varphi$; and vi) (6g) ensures that the Φ fluids are volume filling.

The common pressure feature is not an assumption but a *consequence* of the Lagrangian energy structure and its volume-filling constraint. It can be affected by *algebraic* corrections if for instance interfacial energy or added mass effects are introduced in the Lagrangian [76–78, 97]. However, *dynamically* unequal pressures in a non dissipative system—i.e. involving evolution equations for pressure imbalances—would require adding to the Lagrangian other kinetic and internal energy contributions associated to volume fraction changes of the fluids [75, 97, § 4 eqs 4.13–4.15]. This would produce supplementary evolution equations of Rayleigh–Plesset type.

3.3. Momentum equations

The Euler–Lagrange equations (6) indirectly describe the evolution of velocities (or momenta): they are decomposed into combinations of fields and gradients of Lagrange multipliers (6e), whose time derivatives are defined by the other equations. Eliminating the Lagrange multipliers basically requires that the time derivative of (6e) be combined with gradients of (6c) and (6d). Inspection of (6e) quickly reveals the appropriate linear combination, which, after lengthy but straightforward calculations, yields the evolution equation for the momentum of fluid φ

$$\begin{aligned}&\mathrm{D}_t^\varphi\left([\alpha\rho]^\varphi \times (6\mathrm{e})_i\right) + [\alpha\rho]^\varphi u_{j,i}^\varphi \times (6\mathrm{e})_j - [\alpha\rho]^\varphi \times (6\mathrm{d})_{,i} \\ &\qquad + [\alpha\rho]^\varphi\xi_{,i}^\varphi \times (6\mathrm{c}) - (6\mathrm{b}) \times \psi_{,i}^\varphi - (6\mathrm{a}) \times \phi_{,i}^\varphi \\ &\qquad\qquad \Rightarrow \quad \mathrm{D}_t^\varphi(\alpha^\varphi\rho^\varphi u_i^\varphi) = -\alpha^\varphi P_{,i}\,. \end{aligned} \tag{7}$$

These coupled Euler like equations provide conservation of the total momentum $\sum_\varphi \alpha^\varphi\rho^\varphi\boldsymbol{u}^\varphi$.

$$\textstyle\sum_\varphi (7) \quad \Rightarrow \quad \sum_\varphi \mathrm{D}_t^\varphi(\alpha^\varphi\rho^\varphi u_i^\varphi) = -P_{,i}\,. \tag{8}$$

The notation used to summarize the derivation of the last two equations will be applied throughout this work: any linear operator (sum, product, derivation, gradient, etc.) when applied to one or many equations, is applied to both sides of the equations as exactly given in text by the equation reference—in particular, the order of the left and right-hand sides must be scrupulously preserved.

3.4. Kinetic energy equations

The kinetic energy equation of fluid φ is obtained from the work of the corresponding momentum equation as

$$\begin{aligned}&(7) \times u_i^\varphi - (6\mathrm{a}) \times \tfrac{1}{2}u_i^\varphi u_i^\varphi \\ &\qquad\qquad \Rightarrow \quad \mathrm{D}_t^\varphi(\tfrac{1}{2}\alpha^\varphi\rho^\varphi u_i^\varphi u_i^\varphi) = -\alpha^\varphi P_{,i}u_i^\varphi\,. \end{aligned} \tag{9}$$

Summation over φ yields the equation of total kinetic energy

$$\textstyle\sum_\varphi (9) \quad \Rightarrow \quad \sum_\varphi \mathrm{D}_t^\varphi(\tfrac{1}{2}\alpha^\varphi\rho^\varphi u_i^\varphi u_i^\varphi) = -P_{,i}\overline{u}_i\,, \tag{10}$$

where $\overline{\boldsymbol{u}}$ is the volume averaged velocity

$$\overline{\boldsymbol{u}} = \textstyle\sum_\varphi \alpha^\varphi\boldsymbol{u}^\varphi\,. \tag{11}$$

3.5. Internal energy equations

Under isentropic evolution, the internal energy of fluid φ is a function of the geometric configuration of the system, as defined by the transported density and entropy fields, $e^\varphi = e^\varphi(\rho^\varphi, s^\varphi)$. However, in the dissipative case where entropy is for instance produced by shocks and other physical processes, internal energies must be tracked by evolution equations which

express the fundamental thermodynamic relations along Lagrangian trajectories

$$\mathrm{d}_t^\varphi\, e^\varphi = \frac{P}{(\rho^\varphi)^2}\,\mathrm{d}_t^\varphi\,\rho^\varphi + T^\varphi\,\mathrm{d}_t^\varphi\, s^\varphi\,, \tag{12a}$$

$$\mathrm{d}_t^\varphi\, P = \frac{\gamma^\varphi P}{\rho^\varphi}\,\mathrm{d}_t^\varphi\,\rho^\varphi + \Gamma^\varphi\rho^\varphi T^\varphi\,\mathrm{d}_t^\varphi\, s^\varphi\,. \tag{12b}$$

In order to take into account the common pressure condition explicitly, the system evolution is best expressed through the evolution equation of *pressure in each fluid* φ (12b) which will depend on the associated adiabatic exponent and Grüneisen coefficient, respectively γ^φ and Γ^φ—the isentropic speed of sound is thus given by $c^\varphi = \sqrt{\gamma^\varphi P/\rho^\varphi}$.

The pressure evolution equations (12b) together with mass conservation (6a) can be combined so as to eliminate density derivatives and make appear the sum of volume fraction derivatives

$$\sum_\phi\Big(\frac{\alpha^\phi}{\gamma^\phi}\times(12\mathrm{b}) - \frac{P}{\rho^\phi}\times(6\mathrm{a})\Big)$$

$$\Rightarrow\quad \sum_\phi \frac{\alpha^\phi}{\gamma^\phi}\,\mathrm{d}_t^\phi\, P = -P\sum_\phi \mathrm{D}_t^\phi\,\alpha^\phi + \sum_\phi \frac{\Gamma^\phi}{\gamma^\phi}\alpha^\phi\rho^\phi\mathring{W}^\phi\,, \tag{13}$$

where $\mathring{W}^\varphi = T^\varphi\,\mathrm{d}_t^\varphi\, s^\varphi$ is the per-mass and per-fluid irreversible energy source. Substitution of this pressure derivative eventually yields the fluid density derivative $\mathrm{d}_t^\varphi\,\rho^\varphi$

$$\frac{\alpha^\varphi}{\gamma^\varphi}\times(12\mathrm{b}) - \frac{\alpha^\varphi/\gamma^\varphi}{\sum_\phi \alpha^\phi/\gamma^\phi}\times(13)$$

$$\Rightarrow\quad \sum_\phi \mu^{\varphi\phi}(\mathrm{d}_t^\varphi\, P - \mathrm{d}_t^\phi\, P) = \frac{\alpha^\varphi P}{\rho^\varphi}\,\mathrm{d}_t^\varphi\,\rho^\varphi + \beta^\varphi P\sum_\phi \mathrm{D}_t^\phi\,\alpha^\phi + \sum_\phi \mu^{\varphi\phi}(\Gamma^\varphi\rho^\varphi\mathring{W}^\varphi - \Gamma^\phi\rho^\phi\mathring{W}^\phi)\,, \tag{14}$$

which now does not involve any other *explicit* time derivatives because

$$\sum_\phi \mathrm{D}_t^\phi\,\alpha^\phi = \overline{u}_{i,i}\,, \tag{15a}$$

$$\mathrm{d}_t^\varphi\, P - \mathrm{d}_t^\phi\, P = (u_i^\varphi - u_i^\phi)P_{,i}\,. \tag{15b}$$

These contributions appear in (14) with the respectively global and relative compressibility weighting coefficients which are written in terms of γ^φ or of sound velocities c^φ

$$\beta^\varphi = \frac{\alpha^\varphi/\gamma^\varphi}{\sum_\phi \alpha^\phi/\gamma^\phi} = \frac{\alpha^\varphi/[\rho^\varphi(c^\varphi)^2]}{\sum_\phi \alpha^\phi/[\rho^\phi(c^\phi)^2]}\,, \tag{16a}$$

$$\mu^{\varphi\phi} = \frac{(\alpha^\varphi/\gamma^\varphi)(\alpha^\phi/\gamma^\phi)}{\sum_{\phi'}\alpha^{\phi'}/\gamma^{\phi'}} = \frac{P\alpha^\varphi\alpha^\phi/[\rho^\varphi(c^\varphi)^2\rho^\phi(c^\phi)^2]}{\sum_{\phi'}\alpha^{\phi'}/[\rho^{\phi'}(c^{\phi'})^2]}\,. \tag{16b}$$

The coefficients satisfy the identities $\sum_\varphi\beta^\varphi = 1$, $\sum_\phi\mu^{\varphi\phi} = \alpha^\varphi/\gamma^\varphi$, and $\mu^{\varphi\phi} = \mu^{\phi\varphi} = \beta^\varphi\alpha^\phi/\gamma^\phi = \beta^\phi\alpha^\varphi/\gamma^\varphi$. The energy evolution equation is then obtained as

$$\alpha^\varphi\rho^\varphi\times(12\mathrm{a}) + e^\varphi\times(6\mathrm{a}) - (14)$$

$$\Rightarrow\quad \mathrm{D}_t^\varphi(\alpha^\varphi\rho^\varphi e^\varphi) = -\beta^\varphi P\sum_\phi \mathrm{D}_t^\phi\,\alpha^\phi + \sum_\phi\mu^{\varphi\phi}(\mathrm{d}_t^\varphi\, P - \mathrm{d}_t^\phi\, P) - \sum_\phi\mu^{\varphi\phi}(\Gamma^\varphi\rho^\varphi\mathring{W}^\varphi - \Gamma^\phi\rho^\phi\mathring{W}^\phi) + \alpha^\varphi\rho^\varphi\mathring{W}^\varphi\,, \tag{17}$$

bearing in mind that the Eulerian and Lagrangian derivatives in the right-hand side can but have not been eliminated by substitution with (15): this is deliberate in order to later facilitate the numerical mimicking into (52) to be carried out in Section 4.7. Summation over φ cancels the exchange terms and yields the equation of total internal energy

$$\sum_\varphi(17)\quad\Rightarrow\quad \sum_\varphi \mathrm{D}_t^\varphi(\alpha^\varphi\rho^\varphi e^\varphi) = -P\overline{u}_{i,i} + \sum_\varphi\alpha^\varphi\rho^\varphi\mathring{W}^\varphi\,, \tag{18}$$

which matches the total kinetic energy to yield the conservation of total energy

$$(10)+(18)\quad\Rightarrow\quad \sum_\varphi \mathrm{D}_t^\varphi\,(\alpha^\varphi\rho^\varphi(\tfrac{1}{2}u_i^\varphi u_i^\varphi + e^\varphi)) = -(P\overline{u}_i)_{,i} + \sum_\varphi\alpha^\varphi\rho^\varphi\mathring{W}^\varphi\,. \tag{19}$$

3.6. An important comment on internal energy equations

TO REVIEWERS: This section was separated from the previous in order to highlight an important feature which is not specific to the present derivation and is potentially applicable to any multi-fluid model or scheme.

The derivation of the internal energy equations (17) is an extension of that previously given for $\Phi = 2$ fluids [28, eqs 4 & 5], inspired by previous remarks [98] and calculations [99, 100, resp. eqs 49 & 47]. Many comments therein also hold and are worth being summarized here. This derivation and its consequences are not specific to the present work and are potentially applicable to any other multi-fluid model or scheme.

Multi-fluid studies generally hinge on the evolution equation of per-fluid *total* energy written as

$$\partial_t(\alpha^\varphi\rho^\varphi(\tfrac{1}{2}u_i^\varphi u_i^\varphi + e^\varphi)) + (\alpha^\varphi(\tfrac{1}{2}\rho^\varphi u_i^\varphi u_i^\varphi + \rho^\varphi e^\varphi + P)u_i^\varphi)_{,i} = -P\partial_t\alpha^\varphi + \alpha^\varphi\rho^\varphi\mathring{W}^\varphi\,, \tag{20}$$

in order to make apparent the hyperbolic transport structure on the left-hand side and leave exchange and source terms on the right-hand side. This is achieved at the expense of an *implicit* and *extensive* coupling between *all* the evolution equations and the equations of state through the $\partial_t\alpha^\varphi$ term *alone*.

In contrast, the present evolution equations of per-fluid internal energies (17) *explicitly separate* three different pressure-driven *reversible* processes besides the usual irreversible $\alpha^\varphi\rho^\varphi\mathring{W}^\varphi$: i) $-P\beta^\varphi\overline{u}_{i,i}$ is the internal energy production due to overall volume change; ii) $P_{,i}\sum_\phi\mu^{\varphi\phi}(u_i^\varphi - u_i^\phi)$ is the exchange of internal energy between fluids due to their relative drift along the pressure gradient; and iii) $-\sum_\phi\mu^{\varphi\phi}(\Gamma^\phi\rho^\phi\mathring{W}^\phi - \Gamma^\varphi\rho^\varphi\mathring{W}^\varphi)$ is the *reversible* exchange of internal energy due to differences in *irreversible* heating of fluids. The magnitude of these terms is given by the global and relative compressibility weighting coefficients β^φ and $\mu^{\varphi\phi}$ whose expressions (16) can induce strong stiffness for highly contrasted equations of state: for the common example of air–water mixtures, the ratio $\beta^{\mathrm{Air}}/\alpha^{\mathrm{Air}}$ can reach values in excess of 10^4 when $\alpha^{\mathrm{Air}} \ll 10^{-4}$.

The form (17) of the internal energy equation is thus particularly well suited to understand and design near-isentropic numerical schemes.

3.7. Artificial viscosity

TO REVIEWERS: This section was adapted with simpler and equally robust artificial viscosity closures after (24), with the corresponding changes in the discretized expressions of Section 4.8. The characteristic length scale is now designated as h for consistency with other cell related length scales, appearing and defined for instance in Section 5.

Artificial dissipation is required in order to stabilize shocks in numerical schemes which are insufficiently dissipative [62, 101]: it is thus needed here because GEEC schemes are designed from the onset to be non dissipative up to their order of accuracy. Although it may be viewed as a strictly *numerical* device, artificial dissipation is most often designed by mimicking an explicit *physical* dissipation processes [102]. In single-fluid systems its detailed characteristics are of little importance provided its strength is properly scaled for optimal shock spreading.

For multi-fluid systems in contrast, shocks are not uniquely defined and may depend on the specificities of the actual physical dissipation processes—there are no simple Hugoniot jump relationships—but very few studies have been devoted to analyzing and prescribing expressions for corresponding artificial dissipation. It must be stressed that artificial dissipation here aims at stabilizing the hyperbolic characteristics *alone* thus preserving the elliptic modes.[7] Now, out of the multiplicity of options, multi-fluid dissipation can be designed in a consistent but formally minimal way in order to test schemes or if accurate shock capture is not required. This approach is adopted here following basic concepts previously introduced [25, § 8.3]. Because of the scarceness of similar prescriptions it is detailed below.

Shock stabilization can proceed through many different mechanisms such as shear and volume viscosities, thermal diffusion, inter-fluid drag, and thermal exchange. However, it is known that thermal diffusion *alone* cannot stabilize strong shocks, in contrast to viscosity which is always effective [see for instance 104, § VII.3 and references therein]. Therefore, thermal diffusion will not be retained here although it may improve numerical behavior on some singularities [105].

General shock capture in a multi-fluid system thus requires the presence of a dissipative flux of total momentum in (8), here taken isotropic and designated as the *total* artificial viscosity stress Q

$$\textstyle\sum_\varphi (7) \quad \Rightarrow \quad \sum_\varphi \mathrm{D}_t^\varphi(\alpha^\varphi\rho^\varphi u_i^\varphi) = -P_{,i} - Q_{,i}\,. \tag{21}$$

From there, the momentum equations (7) of fluid φ can always be rewritten as

$$\mathrm{D}_t^\varphi(\alpha^\varphi\rho^\varphi u_i^\varphi) = -\alpha^\varphi P_{,i} - \alpha^\varphi Q_{,i} - \textstyle\sum_\phi D_i^{\varphi\phi}\,, \tag{22}$$

where $\boldsymbol{D}^{\varphi\phi}$ are artificial drag forces coupling fluids φ and ϕ. These terms may correct the differential momentum produced in a shock but will be neglected here as they appear to be only indirectly related to volume changes—characteristic of shocks—and are included in usual physical drag terms—not considered in the present work.

From (22) with $\boldsymbol{D}^{\varphi\phi} = \boldsymbol{0}$, the equation of total kinetic energy (18) is modified as

$$\textstyle\sum_\varphi (22)\times u_i^\varphi$$
$$\Rightarrow \quad \textstyle\sum_\varphi \mathrm{D}_t^\varphi(\frac{1}{2}\alpha^\varphi\rho^\varphi u_i^\varphi u_i^\varphi) = -P_{,i}\overline{u}_i - Q_{,i}\overline{u}_i\,, \tag{23}$$

and, here excluding all other dissipation processes, the dissipative behavior of artificial viscosity now requires that

$$\textstyle\sum_\varphi \alpha^\varphi\rho^\varphi\mathring{W}^\varphi = \overline{\rho}\mathring{W} = -Q\overline{u}_{i,i} \geq 0\,. \tag{24}$$

This condition is always fulfilled if $Q = -\nu\overline{u}_{i,i}$ with $\nu \geq 0$ but i) ν can be any non linear increasing function of strain $\overline{u}_{i,i}$ and ii) the separation of total dissipation into individual fluid dissipations $\mathring{W}^\varphi$ remains open. These points however, can critically impact many applications such as with fluids of highly contrasted equations of state: for instance, shock propagation in a spray of water in air can be significantly affected by changing the dissipation fraction in the much less compressible and denser fluid. For this purpose it is necessary to introduce separate per-fluid artificial viscosity stresses Q^φ whose thermodynamically acceptable closures can vary dramatically in the absence of detailed physical descriptions: extreme cases would be to concentrate dissipation on only one of the fluids φ, thus imposing $Q^\phi = 0$ for any $\phi \neq \varphi$.[8]

Another simple "neutral" two step closure is introduced here. First, the general single-fluid form of artificial viscosity is preserved by setting

$$Q = \overline{\rho}\,\mathcal{Q}[\overline{u}_{i,i}, \overline{c}]\,, \tag{25}$$

where $\overline{\rho} = \sum_\varphi \alpha^\varphi\rho^\varphi$ and $\overline{c}$ are the mean density and the effective speed of sound to be defined. The generic artificial viscosity function $\mathcal{Q}$ combines quadratic and linear contributions according to commonly accepted practice [101]

$$\mathcal{Q}[S, C] = a_2(\min\{0, S\}h)^2 - a_1 CS h\,, \tag{26}$$

where S is an expansion rate, C is a speed of sound, h is the characteristic cell size, and a_1 and a_2 are dimensionless coefficients of order one. Second, the total irreversible work of the artificial viscosity stress (24) is distributed over the fluids in such a way that it does not contribute to *reversible pressure work* in (17), i.e. $\mathring{W}^\varphi$ are such that $\Gamma^\varphi\rho^\varphi\mathring{W}^\varphi = \Gamma^\phi\rho^\phi\mathring{W}^\phi$ for any φ and ϕ. Elementary calculations then show that the irreversible work of the artificial viscosity is distributed according to

$$\alpha^\varphi\rho^\varphi\mathring{W}^\varphi = \lambda^\varphi\overline{\rho}\mathring{W}\,, \qquad \text{with} \qquad \lambda^\varphi = \frac{\alpha^\varphi/\Gamma^\varphi}{\sum_\phi \alpha^\phi/\Gamma^\phi}\,. \tag{27}$$

[7] In an interesting exception [103], artificial viscosity was adapted to only stabilize the elliptic modes at small wavelengths.

[8] In a first version [42, eqs 4.16–18] inspired from previous prescriptions [25, eq. 8.5], the per-fluid artificial viscosity stresses were connected to the per-fluid compression rates and approximated as

$$\alpha^\varphi\rho^\varphi\mathring{W}^\varphi = -\beta^\varphi Q^\varphi\overline{u}_{i,i}\,, \qquad \text{with} \qquad Q^\varphi = -\nu^\varphi\beta^\varphi\overline{u}_{i,i}\,.$$

Following (17), coefficients β^φ were here introduced to formally match the pressure work terms. Although physically sound and plausible, and numerically consistent with the single-fluid scheme in the case of interface cells, this approach was found to be too restrictive on time steps when dealing with small volume fractions of fluids with highly contrasted EOS.

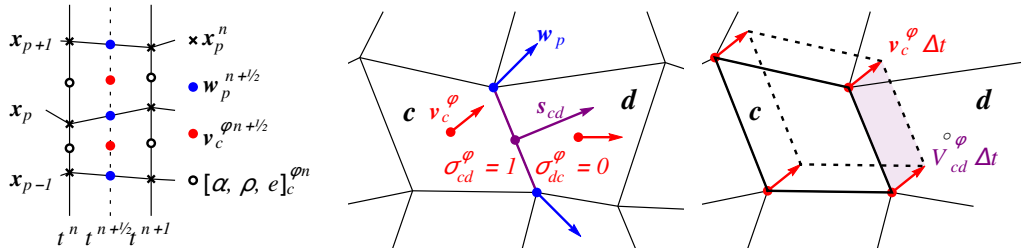

Figure 1: Graphical representations of mesh and discretized quantities in space–time (left) and 2D-space (center), with the swept-flux cell-to-cell transfers (right). Notice the respective node and cell centering of grid and per-fluid relative-to-grid velocities, $\boldsymbol{w}_p^{n+1/2}$ and $\boldsymbol{v}_c^{\varphi n+1/2}$.

4. Derivation of the ALE multi-fluid GEEC scheme

4.1. Discretized fields and action integral

As already mentioned, the present scheme is a multi-fluid extension of a previously developed single-fluid scheme [43] from which, for each fluid's set of fields, it inherits the same discretization choices. These in turn were first selected so as to retain the simple second-order geometric consistency of the von Neumann–Richtmyer scheme [62, 63] (closely related to the Størmer–Verlet integrator) and preserve legacy with existing space- and time-staggered Lagrangian codes [64, 65]. The discretization is described in the following and represented in Fig. 1, but readers are referred to Ref. [43, § 2.2.1] for the underlying rationale.

i) The grid, common to all fluids, is defined at integer-labeled times t^n by nodes labeled p at positions $\boldsymbol{x}_p^n$; ii) According to a fixed connectivity, the nodes delimit polygonal (2D) or polyhedral (3D) cells labeled c with volumes V_c^n; iii) The grid evolution is defined by the velocity of each node $\boldsymbol{w}_p^{n+1/2}$ at half-integer-labeled times as

$$\boldsymbol{w}_p^{n+1/2} = (\boldsymbol{x}_p^{n+1} - \boldsymbol{x}_p^n)/\Delta t^{n+1/2} \,, \tag{28}$$

where $\Delta t^{n+1/2} = t^{n+1} - t^n$; iv) Each fluid possesses its own absolute (in the laboratory frame) velocity $\boldsymbol{u}_c^{\varphi n+1/2}$ and relative-to-grid velocity $\boldsymbol{v}_c^{\varphi n+1/2}$, both defined at half-integer-labeled times but at cell centers and related by

$$\boldsymbol{u}_c^{\varphi n+1/2} = \boldsymbol{w}_c^{n+1/2} + \boldsymbol{v}_c^{\varphi n+1/2} \,, \tag{29}$$

where $\boldsymbol{w}_c^{n+1/2}$ is a mesh velocity interpolated at cell centers from neighboring node values using a simple procedure—for instance arithmetic mean; vi) All other per-fluid quantities—introduced in Section 3.1 for the continuous description—are defined at cells and integer-labeled times as in finite volume approaches: volume fraction $\alpha_c^{\varphi n}$, density $\rho_c^{\varphi n}$, per-mass internal energy $e_c^{\varphi n}$, per-mass entropy $s_c^{\varphi n}$, Lagrangian coordinate $\xi_c^{\varphi n}$, etc. The mass of fluid φ in cell c at time t^n is thus $V_c^n[\alpha\rho]_c^{\varphi n}$.

With the above definitions of discrete fields, a discrete action integral is built as

$$\begin{aligned}
&\text{(1) \& (2)} \\
&\rightsquigarrow \quad \mathcal{A} = \sum_{n,c,\varphi} \Big(\Delta t^{n+1/2} V_c^n \tfrac{1}{2} [\alpha\rho]_c^{\varphi n} (\boldsymbol{u}_c^{\varphi n+1/2})^2 \\
&\qquad - \Delta t^n V_c^n [\alpha\rho]_c^{\varphi n} e^\varphi(\rho_c^{\varphi n}, s^\varphi(\xi_c^{\varphi n})) \\
&\qquad + \phi_c^{\varphi n+1} \, \mathrm{D}_{\Delta t}^\varphi [\alpha\rho]_c^{\varphi n} + \psi_c^{\varphi n+1} \, \mathrm{D}_{\Delta t}^\varphi [\alpha\rho\xi]_c^{\varphi n} \Big) \\
&\qquad - \sum_{n,c} \Pi_c^n \Big(\sum_\varphi \alpha_c^{\varphi n} - 1 \Big) \,,
\end{aligned} \tag{30}$$

which mimics the continuous definition term-to-term—symbol $\rightsquigarrow$ will be used in all the following to relate mimicked equations. The physical meaning of this action integral is thus identical as that introduced and discussed in Sections 2.2 and 3.1, with kinetic and internal energy contributions, conservation constraints for masses and Lagrangian coordinates, and a volume-filling constraint. Important numerical details in (30) are however to be noticed:[9] i) the integral of internal energy is second-order accurate in space and time according respectively to the mid point and trapezium rules as $\Delta t^n = (t^{n+1} - t^{n-1})/2$; ii) the integral of kinetic energy is second-order accurate in space according to the mid point rule, but only first order accurate in time because of the half time-step off-centering of the fluid density—this off-centering is required to match the explicit time discretization of the transport operators discussed below;—iii) the discretization of kinetic energy—and thus momentum—at cell centers does not involve nodal masses and thus complies with the so-called DeBar condition whereby a uniform self-advecting velocity field must remain uniform regardless of density gradients [106, p. 13]; iv) the mass and Lagrangian coordinate constraints are expressed as conservation laws to be rigorously preserved by the discretized transport operators $\mathrm{D}_{\Delta t}^\varphi$ discussed below in Section 4.2; v) the associated Lagrange multipliers must not be viewed as the discretized versions of some continuous fields and have thus been freely labeled in order to best simplify notations in the subsequent Euler–Lagrange equations (38).

4.2. Discrete transport operators

The definition of the so-called "Eulerian" transport operator $\mathrm{D}_{\Delta t}^\varphi$ is a critical ingredient in all the following. It must

[9] Some of these details have evolved compared to earlier [42, § 4.3.2.1 eq. 4.26] and single-fluid versions [43, § 2.2.1 eq. 16].

i) be identical for all conserved fields such as $[\alpha\rho]$ and $[\alpha\rho\xi]$ to simplify later derivations, ii) ensure exact conservation down to round-off errors, and iii) be rigorously positive to preserve physical constraints on $[\alpha\rho]$. For proof of concept and for usage in applications where transport diffusion is not dominant, an explicit first order upwind discretization is here retained to mimic (3a) as

$$\begin{aligned}&\iint_{V_c^{n+1/2},\Delta t^{n+1/2}} (a\,\mathrm{D}_t^\varphi\, b)\,\mathrm{d}^3\boldsymbol{x}\,\mathrm{d}\,t\\ &\rightsquigarrow\quad a_c^{\varphi n+1}\,\mathrm{D}_{\Delta t}^\varphi\, b_c^{\varphi n} = a_c^{\varphi n+1}\Big[V_c^{n+1} b_c^{\varphi n+1} - V_c^n b_c^{\varphi n}\\ &\qquad + \Delta t^{n+1/2}\textstyle\sum_d (\mathring{V}_{cd}^{\varphi n+1/2} b_c^{\varphi n} - \mathring{V}_{dc}^{\varphi n+1/2} b_d^{\varphi n})\Big]\,, \end{aligned}\tag{31}$$

with the definitions for the upwind volume transfer rate from cell c to adjacent cell d

$$\mathring{V}_{cd}^{\varphi n+1/2} = \sigma_{cd}^{\varphi n+1/2}\boldsymbol{s}_{cd}^{n+1/2}\cdot\boldsymbol{v}_c^{\varphi n+1/2}\,,\tag{32a}$$

and the associated upwinding indicator factor (= 0 or 1)

$$\sigma_{cd}^{\varphi n+1/2} = H(\boldsymbol{s}_{cd}^{n+1/2}\cdot\boldsymbol{v}_c^{\varphi n+1/2})\,,\tag{32b}$$

$\boldsymbol{s}_{cd}^{n+1/2}$ being the outward-oriented face-normal surface vector from cell c to adjacent cell d and H being the Heaviside step function. Figure 1 provides a graphical interpretation of this discrete transport operator in terms of swept fluxes.

In all the following unless explicitly denoted, sums $\sum_d$ will be restricted to the adjacent cells d of the nominal current cell c by formally setting $\boldsymbol{s}_{cd}^{n+1/2} = \boldsymbol{0}$ if $c = d$ or if cells c and d do not share any common boundary. Contour integration around the closed boundaries of cells c or d provides the useful relationships

$$\textstyle\sum_c \boldsymbol{s}_{cd}^{n+1/2} = \sum_d \boldsymbol{s}_{cd}^{n+1/2} = \boldsymbol{0}\,.\tag{33}$$

Transport from cell to cell is evidently defined here by the fluids' relative-to-grid velocities alone $\boldsymbol{v}_c^{\varphi n+1/2}$ instead of absolute velocities $\boldsymbol{u}^\varphi$ in (2). In contrast with the implicit transport considered at one point along Ref. [43, eq. 14], transport is here taken explicit: this simplifies the derivations to follow and eventually leads to nearly identical schemes when all operators are corrected to become explicit. Furthermore, whenever the relative-to-grid velocities on two adjacent cells c and d are such that $\sigma_{cd}^{\varphi n+1/2} = \sigma_{cd}^{\varphi n+1/2}$ according to (32b), these upwinding indicator factors must be corrected so as to preserve the relationship

$$\sigma_{cd}^{\varphi n+1/2} + \sigma_{dc}^{\varphi n+1/2} = 1\,,\tag{34}$$

which is necessary condition for consistency of the transport operator [107, eq. 6a]. It must also be noticed that the off-centering of transport operators breaks the Galilean invariance of the action integral towards relative-to-grid motion.

In order to clarify later calculations, it is useful to also mimic the "Lagrangian" transport operator (3b), dual to the direct Eulerian transport through space and time integration by parts: $\int a\,\mathrm{D}_t^\varphi\, b + \int b\,\mathrm{d}_t^\varphi\, a = \int \mathrm{D}_t^\varphi(ab) = \oint(ab)$. Rearranging terms in (31) and neglecting contributions from the space-and-time domain boundary, this simply yields

$$\begin{aligned}&\iint_{V_c^{n+1/2},\Delta t^{n+1/2}} (b\,\mathrm{d}_t^\varphi\, a)\,\mathrm{d}^3\boldsymbol{x}\,\mathrm{d}\,t\\ &\rightsquigarrow\quad b_c^{\varphi n}\,\mathrm{d}_{\Delta t}^\varphi\, a_c^{\varphi n} = b_c^{\varphi n}\Big[V_c^n(a_c^{\varphi n+1} - a_c^{\varphi n})\\ &\qquad + \Delta t^{n+1/2}\textstyle\sum_d \mathring{V}_{cd}^{\varphi n+1/2}(a_d^{\varphi n+1} - a_c^{\varphi n+1})\Big]\,. \end{aligned}\tag{35}$$

With the notations of Ref. [88], one can write $\mathrm{d}_{\Delta t}^\varphi = (\mathrm{D}_{\Delta t}^\varphi)^\flat$ and $\mathrm{D}_{\Delta t}^\varphi = (\mathrm{d}_{\Delta t}^\varphi)^\sharp$. It must be noticed that duality transforms the *explicit upwind* Eulerian operator (31) into an *implicit downwind* Lagrangian operator (35). These definitions however, do not ensure a *local* product rule as visible on the identity

$$\begin{aligned}&a_c^{\varphi n+1}\,\mathrm{D}_{\Delta t}^\varphi\, b_c^{\varphi n} + b_c^{\varphi n}\,\mathrm{d}_{\Delta t}^\varphi\, a_c^{\varphi n} = V_c^{n+1} a_c^{\varphi n+1} b_c^{\varphi n+1} - V_c^n a_c^{\varphi n} b_c^{\varphi n}\\ &\quad + \Delta t^{n+1/2}\textstyle\sum_d (\mathring{V}_{cd}^{\varphi n+1/2} a_d^{\varphi n+1} b_c^{\varphi n} - \mathring{V}_{dc}^{\varphi n+1/2} a_c^{\varphi n+1} b_d^{\varphi n})\\ &\quad \neq \mathrm{D}_{\Delta t}^\varphi(a_c^{\varphi n} b_c^{\varphi n})\,. \end{aligned}\tag{36}$$

The explicit–implicit upwind–downwind duality and the loss of a product rule have major consequences on the variational derivation of the momentum equation—and most notably of its pressure gradient—as shown in Sections 4.4 and 4.5.

4.3. Discrete Euler–Lagrange equations, single pressure condition

The least action principle applied to the discrete system states that the increment equations (or discrete evolution equations) are provided by canceling the variations of the action integral (30) with respect to the discrete field variations

$$\begin{aligned}&(5)\quad\rightsquigarrow\quad \delta\mathcal{A} = \textstyle\sum_{n,c,\varphi}\Big(\dfrac{\partial\mathcal{A}}{\partial\phi_c^{\varphi n+1}}\,\delta\phi_c^{\varphi n+1} + \dfrac{\partial\mathcal{A}}{\partial\psi_c^{\varphi n+1}}\,\delta\psi_c^{\varphi n+1}\\ &\quad + \dfrac{\partial\mathcal{A}}{\partial\xi_c^{\varphi n}}\,\delta\xi_c^{\varphi n} + \dfrac{\partial\mathcal{A}}{\partial[\alpha\rho]_c^{\varphi n}}\,\delta[\alpha\rho]_c^{\varphi n} + \dfrac{\partial\mathcal{A}}{\partial\boldsymbol{v}_c^{\varphi n+1/2}}\cdot\delta\boldsymbol{v}_c^{\varphi n+1/2}\\ &\qquad + \dfrac{\partial\mathcal{A}}{\partial\rho_c^{\varphi n}}\,\delta\rho_c^{\varphi n}\Big) + \textstyle\sum_{n,c}\dfrac{\partial\mathcal{A}}{\partial\Pi_c^n}\,\delta\Pi_c^n = 0\,. \end{aligned}\tag{37}$$

Performing discrete integration by parts and dropping common factors eventually yields

$$(6a)\quad\rightsquigarrow\quad 0 = \mathrm{D}_{\Delta t}^\varphi[\alpha\rho]_c^{\varphi n}\,,\tag{38a}$$

$$(6b)\quad\rightsquigarrow\quad 0 = \mathrm{D}_{\Delta t}^\varphi[\alpha\rho\xi]_c^{\varphi n}\,,\tag{38b}$$

$$(6c)\quad\rightsquigarrow\quad 0 = T_c^{\varphi n}\,\tfrac{\partial s^\varphi}{\partial\xi^\varphi}|_c^n + \mathrm{d}_{\Delta t}^\varphi\,\psi_c^{\varphi n}\,,\tag{38c}$$

$$\begin{aligned}&(6d)\quad\rightsquigarrow\quad 0 = -\Delta t^{n+1/2} V_c^n\,\tfrac{1}{2}(\boldsymbol{u}_c^{\varphi n+1/2})^2 + \Delta t^n V_c^n e_c^{\varphi n} + \Pi_c^n/\rho_c^{\varphi n}\\ &\qquad + \mathrm{d}_{\Delta t}^\varphi\,\phi_c^{\varphi n} + \xi_c^{\varphi n-1}\,\mathrm{d}_{\Delta t}^\varphi\,\psi_c^{\varphi n}\,, \end{aligned}\tag{38d}$$

$$\begin{aligned}&(6e)\quad\rightsquigarrow\quad V_c^n\boldsymbol{u}_c^{\varphi n+1/2} = \textstyle\sum_d \sigma_{cd}^{\varphi n+1/2}\boldsymbol{s}_{cd}^{n+1/2}(\phi_d^{\varphi n+1} - \phi_c^{\varphi n+1}\\ &\qquad + \xi_c^{\varphi n}(\psi_d^{\varphi n+1} - \psi_c^{\varphi n+1}))\,, \end{aligned}\tag{38e}$$

$$(6f)\quad\rightsquigarrow\quad \Pi_c^n = \Delta t^n V_c^n P_c^{\varphi n}\,,\tag{38f}$$

$$(6g)\quad\rightsquigarrow\quad 1 = \textstyle\sum_\varphi \alpha_c^{\varphi n}\,,\tag{38g}$$

which mimics the continuous version, equation to equation. It must be noticed that in order to reach (38e) two important elements are required: i) off-centering factors $\sigma_{cd}^{\varphi n-1/2}$ are not affected by velocity variations $\delta \boldsymbol{v}_c^{\varphi n-1/2}$, i.e. $\partial\sigma^\varphi/\partial\boldsymbol{v}^\varphi = \boldsymbol{0}$, because according to (32b) they are piecewise constant functions of the fluids' relative velocities; and ii) $[\alpha\rho]_c^{\varphi n}$ is factored out because it is specifically matched between the expressions of kinetic energies and transport operators in (30). The $\partial\sigma^\varphi/\partial\boldsymbol{v}^\varphi = \boldsymbol{0}$ assumption may introduce distortions only in the singular Lagrangian limit where $\boldsymbol{v}^\varphi = \boldsymbol{0}$ which generally defines a null subset of the calculation domain.

The close mimicking followed so far makes all the comments in Section 3.2 on the continuous Euler–Lagrange equations (6) to also hold on the discrete equations (38). Particularly noticeable again is that *all fluids share a common pressure field* $P_c^n = \Pi_c^n/(\Delta t^n V_c^n) = P_c^{\varphi n}$, which is the dual relationship to the volume-filling constraint. However, this equal pressure condition may induce numerical constraints depending on EOS stiffness and may thus require specific algorithms beyond the scope of the present study (for instance involving unequal semi-relaxed fluid pressures).

4.4. Variational increment equations of momenta

The close mimicking of the continuous Euler–Lagrange equations (6) by their discrete versions (38) can let believe that the derivation leading to the continuous momentum equation (7) might be similarly mimicked to produce its discrete version. Unfortunately, the simplifications appearing when going from (6) to (7) involve the repeated application of integration by parts and product rule whose discrete versions require specific space-and-time off-centering in order to be exact. The present definitions of operators $\mathrm{D}_{\Delta t}^\varphi$ and $\mathrm{d}_{\Delta t}^\varphi$ in (31) and (35), and the cell indices appearing in the Clebsch decomposition of velocity (38e) do not comply with such requirements. The combination of Euler–Lagrange equations in (7) when applied to (38) produces supplementary *non-conservative non-Galilean-invariant terms which explicitly involve the Lagrange multipliers*.

Three main paths appear in order to circumvent the loss of accurate mimicking: i) seek another combination of the discrete Euler–Lagrange equations which would eliminate all the Lagrange multipliers—but the authors have reservations on the existence of such a combination, fueled by numerous unsuccessful exploratory calculations;—ii) use the full set of discrete Euler–Lagrange equations (38) to simulate the system evolution, instead of the usual discrete Euler equations only—but the Lagrange multipliers evolve through *downwind* transport operators (38c) to (38d) which are known to be highly unstable and would require adding "exotic" artificial dissipation;—or iii) substitute transport and pressure gradient as implicitly contained in (38) by other similar but *consistent, conservative, and Galilean-invariant* operators—error terms with respect to options i) and ii) would be of higher than the operators' order as it appears for instance from (36) and as it was previously analyzed [43]. This last substitution approach will be retained here as it is consistent, simple, and recovers exact Galilean invariance, a highly desirable physical property which is merely approximated to the scheme order in the discrete action integral (30).

Substitution of momentum transport does not require a detailed analysis of how it is embedded in (38) as consistency is preserved by merely adapting the explicit upwind conservative Galilean-invariant transport (31) of the other conserved quantities such as mass and Lagrangian coordinate—detailed 1D single-fluid tests confirmed for instance the marginal impact of the explicit or implicit character of the momentum transport operator [42, §§ 3.5.2 & 3.5.3]. Now, this simple substitution is not applicable to pressure gradients: i) there is no obvious relationship between any of the transport operators and the pressure gradients which could hint at a possible conservative discretization approach; and furthermore ii) in contrast to momentum transport which does not produce work, pressure gradient defines reversible work in internal energy equations and must thus be carefully discretized to preserve thermodynamic consistency. In order to preserve as closely as possible the isentropic (and thus holonomic) character of the discrete momentum equation while restoring its conservation, the contributions to pressure gradient in (7) must be traced, mimicked, and corrected as little as possible.

Inspection of (7) reveals that the pressure gradient arises when eliminating the time derivative of the Lagrange multiplier ϕ^φ through the partial combination of Euler–Lagrange equations $\mathrm{D}_t^\varphi\,([\alpha\rho]^\varphi \times (6\mathrm{e})_i) - [\alpha\rho]^\varphi \times (6\mathrm{d})_{,i} + \cdots$. Its discrete mimicking can be generated by numerous different combinations of (6) but a "canonical" form is found when constraining the combination of discrete equations to: i) produce the Eulerian increment of momentum density $[\alpha\rho]_c^{\varphi n-1}\boldsymbol{u}_c^{\varphi n-1/2}$, ii) fully eliminate the time increments $\phi_c^{\varphi n+1} - \phi_c^{\varphi n}$, and iii) only leave discrete space derivative terms of $\phi_{\{c\}}^{\varphi n+1}$, to be compensated by contributions from the other equations in (6)—similar conditions apply to the discrete elimination of $\psi_c^{\varphi n+1}$ and $\xi_c^{\varphi n+1}$. Therefore, the following expression

$$
\begin{aligned}
&[\alpha\rho]_c^{\varphi n} \times (38\mathrm{e})_c^{n+1/2} - [\alpha\rho]_c^{\varphi n-1} \times (38\mathrm{e})_c^{n-1/2} - [\alpha\rho]_c^{\varphi n-1} \\
&\quad \times \textstyle\sum_d \sigma_{cd}^{\varphi n-1/2} \boldsymbol{s}_{cd}^{n-1/2} \times \big[\ (38\mathrm{d})_d^n/V_d^n - (38\mathrm{d})_c^n/V_c^n\ \big] + \cdots \\
&\Rightarrow \quad V_c^n[\alpha\rho]_c^{\varphi n}\boldsymbol{u}_c^{\varphi n+1/2} - V_c^{n-1}[\alpha\rho]_c^{\varphi n-1}\boldsymbol{u}_c^{\varphi n-1/2} \\
&= -\Delta t^n[\alpha\rho]_c^{\varphi n-1} \textstyle\sum_d \sigma_{cd}^{\varphi n-1/2}\boldsymbol{s}_{cd}^{n-1/2}(e_d^{\varphi n} - e_c^{\varphi n} + P_d^n/\rho_d^{\varphi n} - P_c^n/\rho_c^{\varphi n}) \\
&\qquad\qquad + \text{n.c.t.t.}\,, \qquad (39)
\end{aligned}
$$

is the simplest to match the three conditions: explicit expansion shows that all $\phi_c^{\varphi n}$ terms cancel, only leaving $\phi_c^{\varphi n+1}$. In the second expression, terms involving e^φ and Π are made explicit and all other terms are designated as n.c.t.t. for "non conservative transport terms." Applying discrete Gibbs' equations and product rules, the term on the right-hand side can be transformed according to

$$
\begin{aligned}
&e_d^{\varphi n} - e_c^{\varphi n} + P_d^n/\rho_d^{\varphi n} - P_c^n/\rho_c^{\varphi n} \\
&\quad = P_d^{\varphi n}(\rho_d^{\varphi n} - \rho_c^{\varphi n})/(\rho_d^{\varphi n}\rho_c^{\varphi n}) + T_c^n(s_d^n - s_c^n) + \mathcal{O}[h^2] \\
&\qquad + (P_d^n - P_c^n)/\rho_c^{\varphi n} + P_d^{\varphi n}(\rho_c^{\varphi n} - \rho_d^{\varphi n})/(\rho_d^{\varphi n}\rho_c^{\varphi n}) \\
&\qquad\quad = (P_d^n - P_c^n)/\rho_c^{\varphi n} + T_c^n(s_d^n - s_c^n) + \mathcal{O}[h^2]\,. \qquad (40)
\end{aligned}
$$

The entropy gradients can be dropped as they eventually cancel in combination with (38c). Absorbing all the higher order residues into the non conservative transport terms and approximating to first order in time $[\alpha\rho]_c^{\varphi n-1}/\rho_c^{\varphi n} = \alpha_c^{\varphi n}(1+\mathcal{O}[\Delta t])$—as justified in Section 4.6,—the momentum equation can now be written as

$$V_c^n[\alpha\rho]_c^{\varphi n}\boldsymbol{u}_c^{\varphi n+1/2} - V_c^{n-1}[\alpha\rho]_c^{\varphi n-1}\boldsymbol{u}_c^{\varphi n-1/2} + \text{n.c.t.t.} \\ = -\Delta t^n \alpha_c^{\varphi n}\sum_d \sigma_{cd}^{\varphi n-1/2}\boldsymbol{s}_{cd}^{n-1/2}(P_d^n - P_c^n)\,. \quad (41)$$

Despite the coupling of the fluids through the equal pressure condition (38f), this equation shows that *each fluid* experiences a *separate discrete pressure gradient* which is *downwinded* with respect to its *own velocity*—as already discussed for the special case of the single-fluid scheme [43, § 2.6].

4.5. *Conservative increment equations of momenta, pressure gradient*

TO REVIEWERS: This section was adapted with a simpler and more robust pressure gradient discretization, with the associated changes in the discretized expressions of kinetic and internal energies in Sections 4.6 and 4.7

Conservation of momentum requires pressure gradient terms in the right-hand side of (41) to cancel when summed over some *local* sets of cells c or d and all fluids φ. This is clearly not ensured as off-centering factors can possibly take all combinations of 0 or 1 values depending on relative velocities—the pressure gradient in (41) is not the discrete version of a flux divergence. Just as for the single-fluid scheme [43, § 2.3.2], this must be corrected in the least intrusive way and the privileged approach consists in: i) separating centered contributions, produced by formally setting $\sigma_{cd}^{\varphi n-1/2} = \frac{1}{2}$ and which are naturally conservative, and ii) symmetrizing remaining terms over pairs of neighboring cells. With identity (34) this transforms the pressure gradient into[10]

$$\begin{aligned}
&\textstyle\sum_{\varphi,d}\alpha_c^{\varphi n}\sigma_{cd}^{\varphi n-1/2}\boldsymbol{s}_{cd}^{n-1/2}(P_d^n - P_c^n) \\
&\quad = \textstyle\sum_{\varphi,d}\frac{1}{2}(\alpha_c^{\varphi n} + \alpha_c^{\varphi n}(\sigma_{cd}^{\varphi n-1/2} - \sigma_{dc}^{\varphi n-1/2}))\boldsymbol{s}_{cd}^{n-1/2}(P_d^n - P_c^n) \\
&= \textstyle\sum_{\varphi,d}\frac{1}{2}(\alpha_c^{\varphi n} + \frac{1}{2}(\alpha_c^{\varphi n} + \alpha_d^{\varphi n})(\sigma_{cd}^{\varphi n-1/2} - \sigma_{dc}^{\varphi n-1/2})) \\
&\qquad\qquad \times \boldsymbol{s}_{cd}^{n-1/2}(P_d^n - P_c^n) \\
&\quad + \textstyle\frac{1}{4}\sum_{\varphi,d}(\alpha_c^{\varphi n} - \alpha_d^{\varphi n})(\sigma_{cd}^{\varphi n-1/2} - \sigma_{dc}^{\varphi n-1/2})\boldsymbol{s}_{cd}^{n-1/2}(P_d^n - P_c^n)\,. \quad (42)
\end{aligned}$$

In this last form the first term is conservative because i) for given cells d or c the following respective sums

$$\textstyle\sum_{\varphi,d}\alpha_c^{\varphi n}\boldsymbol{s}_{cd}^{n-1/2}P_c^n = \sum_{\varphi,c}\alpha_c^{\varphi n}\boldsymbol{s}_{cd}^{n-1/2}P_d^n = \boldsymbol{0}\,, \quad (43)$$

cancel thanks to (33), and ii) the off-centered contributions are obviously opposite for each fluid φ over each c–d couple as $(\alpha_c^{\varphi n} + \alpha_d^{\varphi n})(\sigma_{cd}^{\varphi n-1/2} - \sigma_{dc}^{\varphi n-1/2})\boldsymbol{s}_{cd}^{n-1/2}(P_d^n - P_c^n)$ is anti-symmetric through c–d permutation. The last term however, though obviously non conservative, appears to be of higher order $\sum_\varphi \left|\boldsymbol{\nabla}\alpha^\varphi \cdot \boldsymbol{\nabla}P\right|h^4$ than the main term in $\sum_\varphi \|\alpha^\varphi\boldsymbol{\nabla}P\|h^3$: it can thus be safely neglected at the scheme order while preserving the upwind feature produced by the geometric derivation. From (42), the conservative approximation of the total pressure gradient can then be rewritten as

$$\begin{aligned}
&\textstyle\sum_{\varphi,d}\alpha_c^{\varphi n}\sigma_{cd}^{\varphi n-1/2}\boldsymbol{s}_{cd}^{n-1/2}(P_d^n - P_c^n) \\
&\qquad \approx \textstyle\sum_{\varphi,d}\frac{1}{2}(\alpha_c^{\varphi n} + \alpha_d^{\varphi n})\sigma_{cd}^{\varphi n-1/2}\boldsymbol{s}_{cd}^{n-1/2}(P_d^n - P_c^n)\,. \quad (44)
\end{aligned}$$

The final expression of the conservative discrete pressure gradient must now be redistributed on *each* fluid in the least intrusive way, but still according to weights α^φ in order to preserve coupling consistency for any contrasts or gradients of volume fractions. When correcting the pressure gradient according to (44) and substituting the non-conservative transport terms by an explicit upwind conservative operator, the per-fluid momentum increment equation (41) eventually becomes

$$\begin{aligned}
(7) \quad \rightsquigarrow \quad & V_c^n[\alpha\rho]_c^{\varphi n}\boldsymbol{u}_c^{\varphi n+1/2} - V_c^{n-1}[\alpha\rho]_c^{\varphi n-1}\boldsymbol{u}_c^{\varphi n-1/2} \\
&+ \Delta t^{n-1/2}\textstyle\sum_d\left(\mathring{V}_{cd}^{\varphi n-1/2}[\alpha\rho]_c^{\varphi n-1}\boldsymbol{u}_c^{\varphi n-1/2} - \mathring{V}_{dc}^{\varphi n-1/2}[\alpha\rho]_d^{\varphi n-1}\boldsymbol{u}_d^{\varphi n-1/2}\right) \\
&= -\Delta t^n\alpha_c^{\varphi n}\textstyle\sum_d\overline{\sigma}_{cd}^{\varphi n-1/2}\boldsymbol{s}_{cd}^{n-1/2}(P_d^n - P_c^n + Q_d^n - Q_c^n)\,, \quad (45)
\end{aligned}$$

where the corrected upwinding factors are defined as

$$\overline{\sigma}_{cd}^{\varphi n-1/2} = \tfrac{1}{2}\sigma_{cd}^{\varphi n-1/2} + \tfrac{1}{2}\textstyle\sum_\phi\alpha_d^{\phi n}\sigma_{cd}^{\phi n-1/2} \quad (46)$$

and where, following (22), the total artificial viscosity stress Q_c^n has been included—its expression will be given in (56). Just as in the single-fluid case [43, eq. 24], it must be noticed that transport and pressure gradient in (45) involve different time steps, respectively $\Delta t^{n-1/2}$ and Δt^n: this difference is already present in the Euler–Lagrange equation (38d), between the transport of the Lagrange multiplier $\phi_c^{\varphi n}$ and the pressure term, and reflects the initial discretization choice of the action integral in (30). The $\Delta t^{n-1/2}$ factor may appear inappropriate in the increment of velocities centered at half-integer labeled times, but it is perfectly consistent to the scheme order. As of the pressure gradient, it now involves corrected upwinding factors $\sigma_{cd}^{\varphi n-1/2}$ which coincide with the single fluid values [43, eq. 22] in the limit where all α^φ vanish except one, but which, in general are not equal to 0 or 1 and do not verify (34), i.e. $\overline{\sigma}_{cd}^{\varphi n-1/2} + \overline{\sigma}_{dc}^{\varphi n-1/2} \neq 1$. However, it can be shown that (45) still preserves total angular momentum.

At this stage, it is worthwhile commenting on the present derivation of the multi-fluid discrete pressure gradient as compared to previously published procedures. Generally a projection formula is designed to generate discrete quantities from an ideal continuous solution—assumed smooth to some degree or possibly singular. To varying levels, emphasis is then on conservation, monotonicity, consistency, well-posedness and other similar properties which put few constraints on the discretization of the non-conservative pressure terms $-\alpha^\varphi P_{,i}$. Some authors then resort to supplementary and somewhat ad hoc conditions in order to generate "canonical" discrete pressure terms.

[10] The present approach is less intrusive and more robust than a previous one [42, eq. 4.33] which corrected *independently* the per-fluid pressure gradients, with ensuing factors at cell c in (45) that matched $\alpha_c^{\varphi n}$ to the scheme order only.

Two such explicit examples can be cited: i) in Ref. [108, §§ 3.1.1, 3.2.3, and remark 4], by changing the (arbitrary) pressure origin P_0, the balance between flux and exchange terms, $-(\alpha^\varphi(P+P_0))_{,i}$ and $\alpha^\varphi_{,i}(P+P_0)$, is modified and enables using a discretization procedure that demands the well-posedness of the truncated conservative equations; ii) in Ref. [31, § 2.2 and Fig. 3], the scheme is forced to match the discretization of a separated flow where volume fractions behave as a supplementary "internal" dimension. Here, in contrast, the preeminence of thermodynamic consistency for isentropic evolution effectively lifts all ambiguities on the pressure gradient discretization, even if corrections to the scheme order are added to recover exact conservation. The observed impact of the ensuing pressure downwinding is consistent with previous observations showing that the low Mach behavior of single-fluid schemes is improved by pressure gradient centering [109, § 5.3] or by the implicit downwinding embedded in Lagrange-plus-Remap approaches [110–112].

4.6. Increment equations of kinetic energies

The increment equation of per-fluid kinetic energy is obtained from the momentum increment equation and, after lengthy but straightforward calculations, gives

$$
\begin{aligned}
(9) \quad \rightsquigarrow \quad & (45)\cdot\tfrac{1}{2}(\boldsymbol{u}_c^{\varphi n+1/2}+\boldsymbol{u}_c^{\varphi n-1/2})-(38\mathrm{a})^{n-1}\times\tfrac{1}{2}(\boldsymbol{u}_c^{\varphi n+1/2}\cdot\boldsymbol{u}_c^{\varphi n-1/2})\\
\Rightarrow \quad & V_c^n\tfrac{1}{2}[\alpha\rho]_c^{\varphi n}(\boldsymbol{u}_c^{\varphi n+1/2})^2-V_c^{n-1}\tfrac{1}{2}[\alpha\rho]_c^{\varphi n-1}(\boldsymbol{u}_c^{\varphi n-1/2})^2\\
&+\Delta t^{n-1/2}\textstyle\sum_d\big(\mathring{V}_{cd}^{\varphi n-1/2}\tfrac{1}{2}[\alpha\rho]_c^{\varphi n-1}(\boldsymbol{u}_c^{\varphi n-1/2})^2\\
&\qquad-\mathring{V}_{dc}^{\varphi n-1/2}\tfrac{1}{2}[\alpha\rho]_d^{\varphi n-1}(\boldsymbol{u}_d^{\varphi n-1/2})^2\big)\\
&+\Delta t^{n-1/2}\textstyle\sum_d\mathring{V}_{dc}^{\varphi n-1/2}\tfrac{1}{2}[\alpha\rho]_d^{\varphi n-1}\\
&\qquad(\boldsymbol{u}_c^{\varphi n+1/2}-\boldsymbol{u}_d^{\varphi n-1/2})\cdot(\boldsymbol{u}_c^{\varphi n-1/2}-\boldsymbol{u}_d^{\varphi n-1/2})\\
=\ & -\Delta t^n\alpha_c^{\varphi n}\tfrac{1}{2}\textstyle\sum_d\overline{\sigma}_{cd}^{\varphi n-1/2}\boldsymbol{s}_{cd}^{n-1/2}\cdot(\boldsymbol{u}_c^{\varphi n+1/2}+\boldsymbol{u}_c^{\varphi n-1/2})\\
&\qquad\times(P_d^n-P_c^n+Q_d^n-Q_c^n)\\
=\ & -\Delta t^n\alpha_c^{\varphi n}(\langle\boldsymbol{u}^\varphi\cdot\boldsymbol{\nabla}P\rangle_c^n+\langle\boldsymbol{u}^\varphi\cdot\boldsymbol{\nabla}Q\rangle_c^n)\,, \qquad (47)
\end{aligned}
$$

with the following definition which will simplify later calculations

$$
\langle\boldsymbol{u}^\varphi\cdot\boldsymbol{\nabla}P\rangle_c^n=\tfrac{1}{2}\textstyle\sum_d\overline{\sigma}_{cd}^{\varphi n-1/2}(\boldsymbol{u}_c^{\varphi n+1/2}+\boldsymbol{u}_c^{\varphi n-1/2})\cdot\boldsymbol{s}_{cd}^{n-1/2}(P_d^n-P_c^n)\,. \qquad (48)
$$

The term on the right-hand side of (47) is simply the work of pressure forces and is to be matched by opposite terms in the internal energy equations. On the left-hand side, the transport of kinetic energy was separated into the common transport operator of conserved quantities and a numerical residue. The residue is quadratic in velocity and from its canonical form

$$
\begin{aligned}
&(\boldsymbol{u}_c^{\varphi n+1/2}-\boldsymbol{u}_d^{\varphi n-1/2})\cdot(\boldsymbol{u}_c^{\varphi n-1/2}-\boldsymbol{u}_d^{\varphi n-1/2})\\
&=\tfrac{1}{4}(\boldsymbol{u}_c^{\varphi n+1/2}+\boldsymbol{u}_c^{\varphi n-1/2}-2\boldsymbol{u}_d^{\varphi n-1/2})^2-\tfrac{1}{4}(\boldsymbol{u}_c^{\varphi n+1/2}-\boldsymbol{u}_c^{\varphi n-1/2})^2\,, \qquad (49)
\end{aligned}
$$

its sign is found positive for small enough values of time step Δt^n: as already established [113, § 7], explicit discrete transport of momentum dissipates kinetic energy under CFL condition.

Finally the increment equation of total kinetic energy is found as

$$
\begin{aligned}
(10) \quad \rightsquigarrow \quad & \textstyle\sum_\varphi(47)\\
\Rightarrow \quad & V_c^n\textstyle\sum_\varphi\tfrac{1}{2}[\alpha\rho]_c^{\varphi n}(\boldsymbol{u}_c^{\varphi n+1/2})^2-V_c^{n-1}\sum_\varphi\tfrac{1}{2}[\alpha\rho]_c^{\varphi n-1}(\boldsymbol{u}_c^{\varphi n-1/2})^2\\
&+\Delta t^{n-1/2}\textstyle\sum_{\varphi,d}\big(\mathring{V}_{cd}^{\varphi n-1/2}\tfrac{1}{2}[\alpha\rho]_c^{\varphi n-1}(\boldsymbol{u}_c^{\varphi n-1/2})^2\\
&\qquad-\mathring{V}_{dc}^{\varphi n-1/2}\tfrac{1}{2}[\alpha\rho]_d^{\varphi n-1}(\boldsymbol{u}_d^{\varphi n-1/2})^2\big)\\
&+\Delta t^{n-1/2}\textstyle\sum_{\varphi,d}\mathring{V}_{dc}^{\varphi n-1/2}\tfrac{1}{2}[\alpha\rho]_d^{\varphi n-1}(\boldsymbol{u}_c^{\varphi n+1/2}-\boldsymbol{u}_d^{\varphi n-1/2})\\
&\qquad\cdot(\boldsymbol{u}_c^{\varphi n-1/2}-\boldsymbol{u}_d^{\varphi n-1/2})\\
=\ & -\Delta t^n\tfrac{1}{2}\textstyle\sum_{\varphi,d}\alpha_c^{\varphi n}\overline{\sigma}_{cd}^{n-1/2}\boldsymbol{s}_{cd}^{n-1/2}\cdot(\boldsymbol{u}_c^{\varphi n+1/2}+\boldsymbol{u}_c^{\varphi n-1/2})\\
&\qquad\times(P_d^n-P_c^n+Q_d^n-Q_c^n)\,. \qquad (50)
\end{aligned}
$$

4.7. Increment equations of internal energies

As already introduced in Section 2.3, designing the scheme's increment equations for internal energies requires: i) balancing the increment equations of kinetic energies in order to achieve energy conservation, ii) mimicking the (continuous) evolution equations of internal energies, here in explicit form (17), and iii) producing the highest order of approximation compatible with both the first two constraints and an acceptable level of algorithmic complexity. This approach could be carried out to second order in previous studies of Lagrangian space- and time-staggered schemes [64] and of the variational direct ALE single-fluid version of the present scheme [43]. As a first step, because of the complexities of the internal energy couplings and because the scheme order is already limited by the first order discretization of transport, we shall here apply the procedure on a low order but simple explicit time discretization.

Inspection of (17) and (9)—complemented with (10) and (11)—reveals how the correspondence between the various pressure work terms can be applied here to (50). First, the mean expansion $\overline{u}_{i,i}$ appears as dual to the pressure work $P_{,i}\overline{u}_i$ in the total kinetic energy equation(10). Thus, factorizing terms in P_c^n from the whole domain which are present at the right-hand side of (50) yields the compatible discrete mean volume derivative

$$
\begin{aligned}
(15\mathrm{a}) \quad \rightsquigarrow \quad \langle\mathring{V}\rangle_c^n=\ & \tfrac{1}{2}\textstyle\sum_{\varphi,d}\boldsymbol{s}_{cd}^{n-1/2}\cdot[\alpha_c^{\varphi n}\overline{\sigma}_{cd}^{n-1/2}(\boldsymbol{u}_c^{\varphi n+1/2}+\boldsymbol{u}_c^{\varphi n-1/2})\\
&+\alpha_d^{\varphi n}\overline{\sigma}_{dc}^{n-1/2}(\boldsymbol{u}_d^{\varphi n+1/2}+\boldsymbol{u}_d^{\varphi n-1/2})]\,. \qquad (51)
\end{aligned}
$$

Next, the Lagrangian drift derivatives $u_i^\varphi P_{,i}$ appear in the kinetic energy equation (9). From (47) by energy conservation, it is thus straightforward to build the following increment equation of internal energy

$$
\begin{aligned}
(17) \quad \rightsquigarrow \quad & V_c^{n+1}[\alpha\rho]_c^{\varphi n+1}e_c^{\varphi n+1}-V_c^n[\alpha\rho]_c^{\varphi n}e_c^{\varphi n}\\
&+\Delta t^{n+1/2}\textstyle\sum_d\big(\mathring{V}_{cd}^{\varphi n+1/2}[\alpha\rho]_c^{\varphi n}e_c^{\varphi n}-\mathring{V}_{dc}^{\varphi n+1/2}[\alpha\rho]_d^{\varphi n}e_d^{\varphi n}\big)\\
=\ & -\Delta t^n\beta_c^{\varphi n}P_c^n\langle\mathring{V}\rangle_c^n\\
&\qquad+\Delta t^n\textstyle\sum_\phi\mu_c^{\varphi\phi n}(\langle\boldsymbol{u}^\varphi\cdot\boldsymbol{\nabla}P\rangle_c^n-\langle\boldsymbol{u}^\phi\cdot\boldsymbol{\nabla}P\rangle_c^n)\\
&\qquad-\textstyle\sum_\phi\mu_c^{\varphi\phi n}(\Gamma_c^{\varphi n}\langle\rho^\varphi\,\delta W^\varphi\rangle_c^n-\Gamma_c^{\phi n}\langle\rho^\phi\,\delta W^\phi\rangle_c^n\\
&\qquad\qquad+\alpha_c^{\varphi n}\langle\rho^\varphi\,\delta W^\varphi\rangle_c^n\,, \qquad (52)
\end{aligned}
$$

where notations (51) and (48) have been used and dissipation contributions from artificial viscosity and numerical transport of kinetic energy have been regrouped as

$$\begin{aligned}\alpha_c^{\varphi n}\langle\rho^\varphi\,\delta W^\varphi\rangle_c^n &= -\Delta t^n \lambda_c^{\varphi n} Q_c^n \langle\mathring{V}\rangle_c^n \\ &\quad + \Delta t^{n-1/2}\textstyle\sum_d \mathring{V}_{dc}^{\varphi n-1/2}\frac{1}{2}[\alpha\rho]_d^{\varphi n-1} \\ &\quad \times (\boldsymbol{u}_c^{\varphi n+1/2}-\boldsymbol{u}_d^{\varphi n-1/2})\cdot(\boldsymbol{u}_c^{\varphi n-1/2}-\boldsymbol{u}_d^{\varphi n-1/2})\,, \end{aligned} \tag{53}$$

with

$$(27) \quad \rightsquigarrow \quad \lambda_c^{\varphi n} = \frac{\alpha_c^{\varphi n}/\Gamma_c^{\varphi n}}{\sum_\phi \alpha_c^{\phi n}/\Gamma_c^{\phi n}}\,. \tag{54}$$

At this stage, some important features of the increment equation of internal energy (52) must be highlighted and commented: i) mimicking of the global volume rate of change $\overline{u}_{i,i}$ in (51) is relatively straightforward and, being dual of a downwinded $P_{,i}$, it is necessarily *upwinded*; ii) mimicking of the drift induced pressure work $(u_i^\varphi - u_i^\phi)P_{,i}$ is less trivial and must combine the *per-fluid downwinded* $P_{,i}$ because, as visible in (15b), it involves per-fluid Lagrangian (not Eulerian) time derivatives of P; iii) as already mentioned above, it is *explicit*—thus avoiding a complex *non-linear, non-local, and implicit* coupling between internal energies of *all the fluids*, formally written as

$$e_c^{\varphi n+1} = e_c^{\varphi n} \cdots - \textstyle\sum_{\phi,d}\langle\Delta V\rangle_d^{\phi n}\mathcal{P}^\phi(e_d^{\phi n+1})\,, \tag{55}$$

as shown by inspection of (52);—iv) it is thus first order accurate in time with the corresponding reduction in the accuracy of isentropic behavior—in contrast to what was achieved in the single-fluid case [43]; and v) in principle, the mimicking procedure should still be applicable when crafting an explicit second-order scheme based on a prediction–correction approach [64, 65]. This last option will be explored in later publications.

4.8. Discrete artificial viscosity

Mimicking of artificial viscosity as discussed in Section 3.7 does not raise any major issues. Criteria to select coefficients and shock spreading length, a_2, a_1, and h_c^n, have been already explored and reviewed at length [101, see for instance], and their extension to the present multi-fluid case will not be further discussed here: in general $a_2 \approx a_1 \approx 0.5$, and h_c^n can be identified with the cell size used for CFL estimation as in Section 5.1.

The discrete artificial viscosity stress is thus defined by mimicking as

$$(25) \quad \rightsquigarrow \quad Q_c^n = \overline{\rho}_c^n \mathcal{Q}[\langle\mathring{V}\rangle_c^{n-1/2}/V_c^n, c_c^n]\,. \tag{56}$$

where $\mathcal{Q}$ is given by (26). Because according to (51) computation of $\langle\mathring{V}\rangle_c^n$ requires knowledge of the velocity field at time $t^{n+1/2}$ which in turn requires knowledge of Q_c^n, the volume rate of change in (56) was adapted into

$$\langle\mathring{V}\rangle_c^{n-1/2} = \textstyle\sum_{\varphi,d}\boldsymbol{s}_{cd}^{n-1/2}\cdot(\alpha_c^{\varphi n}\overline{\sigma}_{cd}^{n-1/2}\boldsymbol{u}_c^{\varphi n-1/2} + \alpha_d^{\varphi n}\overline{\sigma}_{dc}^{n-1/2}\boldsymbol{u}_d^{\varphi n-1/2})\,. \tag{57}$$

Again, a prediction–correction approach can correct this approximation to the scheme order and widen the CFL stability range as was previously shown for Lagrangian schemes [64, 65].

4.9. Pressure, densities, and volume fractions

At the end of the cycle, both $[\alpha\rho]_c^{\varphi n+1}$ and $e_c^{\varphi n+1}$ are available by solving (38a) and (52) respectively, but $\alpha_c^{\varphi n+1}$, $\rho_c^{\varphi n+1}$, and P_c^{n+1} need to be computed. The last two quantities are simultaneously obtained by solving the *local* system of $\Phi+1$ (non linear) equations in the $\Phi+1$ variables ρ^φ and P

$$\mathcal{P}^\varphi(\rho^\varphi, e^\varphi) = P\,, \tag{58a}$$

$$\textstyle\sum_\varphi[\alpha\rho]^\varphi/\rho^\varphi = 1\,, \tag{58b}$$

where $\mathcal{P}^\varphi$ are the pressure parts of the fluids' equations of state, and time and cell indices have been dropped here for simplicity.

It must be stressed that, in contrast to many other multi-fluid schemes which require entropic pressure relaxation procedures [114], this step does not modify internal energies through neither reversible nor irreversible processes. The thermodynamically consistent evolution of energies is completely captured to the scheme order by (52) and e^φ are thus known and fixed in (58). Excluding single calls to the thermodynamic coefficients γ^φ and Γ^φ, (58) is the only place in the scheme where equations of state are called: this convenient feature is a direct consequence of the explicit form of the energy equations.

The system (58) has simple explicit solutions for mixtures of different Tammann's "stiffened" gases for which (see [115, eqs 7.31–7.35] for a rationale on notations)

$$\mathcal{P}^\varphi(\rho^\varphi, e^\varphi) = \Gamma^\varphi\rho^\varphi e^\varphi - \pi^\varphi\,, \tag{59}$$

with Γ^φ and π^φ constant but with only one or two different offset pressures π^φ for $1 \le \varphi \le \Phi$, possibly degenerated into perfect gases when $\pi^\varphi = 0$—notice here that in general $\gamma^\varphi = \Gamma^\varphi + 1 + \pi^\varphi/P \neq \Gamma^\varphi + 1$ is pressure dependent, equality holding for perfect gases only. For two common offset pressures π^1 and π^2 and labeling the two corresponding subsets of φ by sub-subscripts $m = 1$ and 2, it is found

$$\rho^{\varphi_m} = \frac{P+\pi^m}{\Gamma^{\varphi_m}e^{\varphi_m}}\,, \tag{60a}$$

$$\alpha^{\varphi_m} = \frac{\Gamma^{\varphi_m}[\alpha\rho]^{\varphi_m}e^{\varphi_m}}{P+\pi^m}\,, \tag{60b}$$

where P is solution of the 2nd degree equation

$$1 = \frac{\sum_{\varphi_1}\Gamma^{\varphi_1}[\alpha\rho]^{\varphi_1}e^{\varphi_1}}{P+\pi^1} + \frac{\sum_{\varphi_2}\Gamma^{\varphi_2}[\alpha\rho]^{\varphi_2}e^{\varphi_2}}{P+\pi^2}\,. \tag{60c}$$

For one common offset pressure $\pi^1 = \pi^2 = \pi$, equations (60) hold, with the last (60c) simplified into

$$P = \textstyle\sum_\varphi\Gamma^\varphi[\alpha\rho]^\varphi e^\varphi - \pi\,, \tag{61}$$

For more elaborated or numerous equations of state—which are beyond the scope of this work—(58) can be solved using an iterative Newton–Raphson method. Improved convergence of the algorithm can be achieved by providing a good estimate of $\rho_c^{\varphi n+1}$ as initial value, for instance produced with the discrete version of (14) analogous to (52) for internal energies.

5. Summary of the GEEC multi-fluid ALE scheme

5.1. Time step

The time step of the simulation $\Delta t^{n+1/2}$ is bounded by an approximate but simple CFL condition involving the fluids' relative-to-grid velocities and the upper bound of the sound velocity of the mixture c_c^n according to

$$\Delta t^{n+1/2} = \mathrm{CFL} \times \min_{\varphi,c} \{h_c^n/(c_c^n + |\boldsymbol{v}_c^{\varphi n-1/2}|)\} \,, \tag{62}$$

where h_c^n is a characteristic length scale of cell c at time t^n, also used to scale artifical viscosity in (56) with (26)—here for a quadrilateral, h_c^n is the smallest of the diagonal and median lengths. In any mixed system the upper bound of the sound velocity is obtained when all dissipation processes vanish—i.e. at zero drag force and zero thermal exchange—and can be expressed using the sound velocities of the fluids and the compressibility weighting coefficients (16a) according to [58]

$$(c_c^n)^2 = \textstyle\sum_\varphi \beta_c^{\phi n} (c_c^{\varphi n})^2 \,, \quad \text{with} \quad (c_c^{\varphi n})^2 = \gamma_c^{\varphi n} P_c^n / \rho_c^{\varphi n} \,. \tag{63}$$

For more streamlined calculations the time-step limitation should also take into account all the other potential sources of numerical stiffness, in particular those of the energy equations as visible in (17). In its present form however, (62) with CFL ≈ 0.25 was found sufficient to carry out all the tests reported in Section 6.

5.2. Near-Lagrangian grid velocity

As the grid velocity $\boldsymbol{w}$ and the absolute velocities of fluids $\boldsymbol{u}^\varphi$ are not discretized over identical elements, an interpolation or averaging procedure must be applied in order to compute a near-Lagrangian grid velocity for usage in grid evolution prescriptions.

Following the strategy elaborated in Ref. [43, App. B], a near-Lagrangian grid velocity can be obtained by minimizing the quadratic total volume flux over the cell edges (c,d) neighboring each node p of the grid, yielding

$$\boldsymbol{w}_p^{\mathrm{NL}\ n+1/2} = \arg\min_{\boldsymbol{w}} \textstyle\sum_{\varphi,(c,d)\in\mathcal{C}(p)} \left(\alpha_c^{\varphi n} \boldsymbol{s}_{cd}^{n+1/2} \cdot (\boldsymbol{u}_c^{\varphi n+1/2} - \boldsymbol{w})\right)^2 \,, \tag{64}$$

where $\boldsymbol{u}_c^{\varphi n+1/2}$ is the absolute fluid velocity given by the scheme. The sum over fluids φ is here carried out with α^φ weights over $1 \le \varphi \le \Phi$, but could be differently weighted or restricted to fewer or even just one φ depending on the grid evolution strategy defined by the user. Equation 64 is implicit and nonlocal as knowledge of $\boldsymbol{w}_p^{n+1/2}$ is required in order to calculate $\boldsymbol{s}_{cd}^{n+1/2}$. An iterative procedure could be used—possibly with stability and convergence issues—but in all the tested applications a first order approximation obtained by replacing $\boldsymbol{s}_{cd}^{n+1/2}$ by $\boldsymbol{s}_{cd}^n$ was found satisfactory. Second-order accuracy can be obtained by a prediction–correction approach.

Taking the derivative of (64) with respect to $\boldsymbol{w}$ yields

$$\textstyle\sum_{\varphi,(c,d)\in\mathcal{C}(p)} (\alpha_c^{\varphi n})^2 (\boldsymbol{s}_{cd}^{n+1/2} \otimes \boldsymbol{s}_{cd}^{n+1/2}) \cdot (\boldsymbol{u}_c^{\varphi n+1/2} - \boldsymbol{w}_p^{\mathrm{NL}\ n+1/2}) = \boldsymbol{0} \,, \tag{65}$$

which can be written under the final formulation

$$\boldsymbol{w}_p^{\mathrm{NL}\ n+1/2} = \Big(\textstyle\sum_{\varphi,(c,d)\in\mathcal{C}(p)} (\alpha_c^{\varphi n})^2 (\boldsymbol{s}_{cd}^{n+1/2} \otimes \boldsymbol{s}_{cd}^{n+1/2}) \Big)^{-1} \cdot \Big(\textstyle\sum_{\varphi,(c,d)\in\mathcal{C}(p)} (\alpha_c^{\varphi n})^2 (\boldsymbol{s}_{cd}^{n+1/2} \otimes \boldsymbol{s}_{cd}^{n+1/2}) \cdot \boldsymbol{u}_c^{\varphi n+1/2} \Big) \,. \tag{66}$$

The actual grid velocity can then be defined through some prescribed function as $\boldsymbol{w}_p^{n+1/2} = \mathcal{W}(\{\boldsymbol{w}_p^{\mathrm{NL}\ n+1/2}\})$.

5.3. Summary of iteration cycle, basic properties

The multi-fluid GEEC scheme solves the evolution equations for mass, momentum, and internal energy of each fluid, respectively (6a), (7), and (17). Starting from the main quantities at time t^n, the scheme's elementary time step to t^{n+1} consists in the successive application of increment equations as schematized in Table 2.

Boundary conditions have not been discussed in the present work as they can take a very wide variety of types in multi-fluid systems and are generally rather simple to implement in a first order explicit scheme—for instance through ghost cells. Tests in Section 6 involved basically perfect walls or static homogeneous states at infinity.

As reflected in the notations, the scheme is applicable in any number of dimensions on any type and structure of time dependent (ALE) mesh with *constant connectivity*. This last constraint can be relaxed (with heavier notations) as it is not necessary in order to properly define a discrete action integral.

The scheme is formally of second order in space and time in the Lagrangian limit but first order for relative-to-grid transport and its associated terms.

6. Two-dimensional numerical results

6.1. Comments on test selection

Extensive benchmarking of the present numerical scheme with all its specific and numerous features is beyond the scope of the present work. Three test cases are just provided here as illustrations. The first two are Sod's shock tube and Ransom's faucet which are retained for being de facto mandatory benchmarks in the communities of compressible single- and two-fluid CFD, but are here adapted to deliberately stress the scheme in its 2D ALE features. The third is an original eight-clouds-crossing test specifically designed to simultaneously and strenuously probe the compressible high-speed high-contrast multi-fluid ALE features as can be found in some extreme applications. An animation of this last test is available as supporting information on the journal website. Various others tests were also carried out [42, § 4.5] with another but almost identical scheme, only differing by high-order numerical residues in the energy equation.

In all test cases, fluids represent for instance air or water as described by equation of state (59), for respectively perfect or stiffened gas, with commonly accepted coefficients $\pi^{\mathrm{Air}} = 0$ and $\Gamma^{\mathrm{Air}} = 2/5$ $(= \gamma^{\mathrm{Air}} - 1)$, and $\pi^{\mathrm{Water}} = 21 \times 10^8$ Pa and $\Gamma^{\mathrm{Water}} = 6$. Initial densities at ambient pressure $P = 10^5$ Pa will be $\rho^{\mathrm{Air}} = 1$ kg.m^{-3} and $\rho^{\mathrm{Water}} = 10^3$ kg.m^{-3}

At t^n	$\Delta t^{n-1/2}$	$\boldsymbol{u}_c^{\varphi n-1/2}$	$\boldsymbol{w}_p^{n-1/2}$	$\boldsymbol{x}_p^n$	$\boldsymbol{v}_c^{\varphi n-1/2}$	$\sigma_{cd}^{\varphi n-1/2}$	$[\alpha\rho]_c^{\varphi n}$	$e_c^{\varphi n}$	$\alpha_c^{\varphi n}$	$\rho_c^{\varphi n}$	P_c^n	$Q_c^{\varphi n}$
(62)	$\Delta t^{n+1/2}$											
(45)		$\boldsymbol{u}_c^{\varphi n+1/2}$										
e.g. (66) & (28)			$\boldsymbol{w}_p^{n+1/2}$	$\boldsymbol{x}_p^{n+1}$								
(29) & (32b)					$\boldsymbol{v}_c^{\varphi n+1/2}$	$\sigma_{cd}^{\varphi n+1/2}$						
(38a)							$[\alpha\rho]_c^{\varphi n+1}$					
(52)								$e_c^{\varphi n+1}$				
(58)									$\alpha_c^{\varphi n+1}$	$\rho_c^{\varphi n+1}$	P_c^{n+1}	
(56)												$Q_c^{\varphi n+1}$

Table 2: List of increment equations to be successively applied (left column, from top to bottom) in order to complete one time step of the present multi-fluid ALE scheme: from the values at t^n (top line), the final values at t^{n+1} appear successively over the time step.

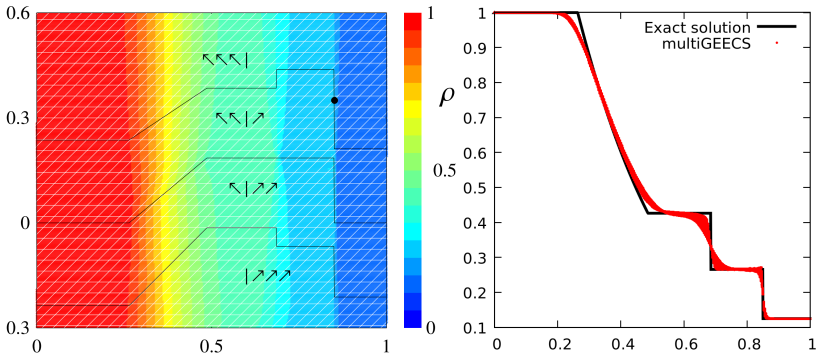

(a) Density map (b) Superposed density profiles along x

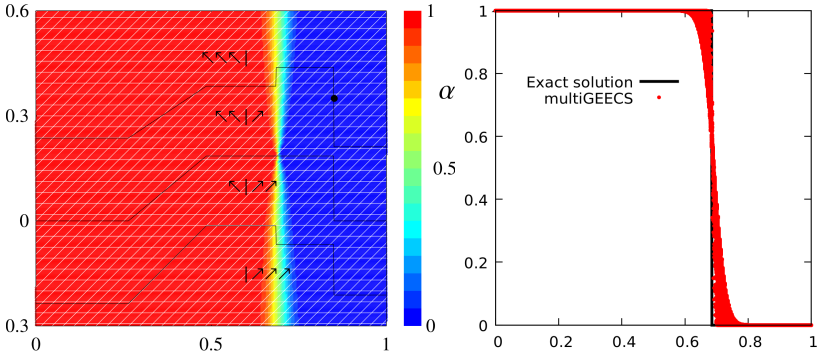

(c) Volume fraction map (d) Superposed volume fraction profiles along x

Figure 2: Density (top) and volume fraction (bottom) maps and profiles for the two-dimensional two-fluid Sod's shock tube computed with the present GEEC multi-fluid scheme on grid sheared across the x direction. Grid velocity is $w_x = 5y$ and $w_y = 0$ and is thus supersonic over bottom and top zones of the domain. Black lines on density maps are loci of points where grid moves at material and sonic velocities $w_x = u_x$ and $w_x = u_x \pm c$. At the black dot, grid and shock velocities match. CFL = 0.5, 320×290 cells, one in ten grid lines represented in both dimensions (white lines).

6.2. Sod's shock tube variant: two-dimensional, sheared ALE grid, two-fluid

Sod's shock tube [116] is a simple 1D Riemann problem on a perfect gas at $\Gamma = \gamma - 1 = 2/5$ with initial left and right states specified as

	$\rho^{\pm}$	P	$\boldsymbol{u}^{\pm}$	α^+	α^-	(67)
$x < 1/2$	1	1	0	$1 - 10^{-12}$	10^{-12}	
$x > 1/2$	1/8	1/10	0	10^{-12}	$1 - 10^{-12}$	

Its analytical solution consists in three waves: a shock, a contact discontinuity, and an expansion fan. It is generally used to test the one-dimensional behavior of numerical schemes, mostly on Eulerian or Lagrangian grids.

Two-dimensional variants of Sod's shock tube test were reported for the single-fluid versions of the present GEEC scheme [43, § 4.3 and Fig. 5]. While keeping the physical 1D plane symmetry of the flow, they intended to reveal possible numerical distortions from deliberately non-symmetric ALE mesh

evolution, there taken as simple shears along the x or y axis. This produced highly non-uniform fluid motions *relative to the grid*, from quasi-Lagrangian to supersonic, whose impact could be deleterious on a possibly inconsistent integration of internal energy. This strategy of grid shearing is even more relevant in the present multi-fluid context of simultaneous integration of coupled internal energy equations and will thus be adopted here. As in Ref. [43, § 4.3] the calculation domain is $[0; 1] \times [-0.3; 0.6]$ and the grid velocity is $w_x = 5y$ and $w_y = 0$, with maximal and minimal values of respectively $w_x = 3$ at $y = 0.6$ and $w_x = -1.5$ at $y = -0.3$. As illustrated in Fig. 2a, the grid then undergoes a shearing across the x direction with a shifting of the characteristics. The domain is meshed into 320×290 initially square cells which become parallelograms with a $\pi/4$ tilt at final time $t = 0.2$.

The test is here further expanded into a two-fluid variant, where the left and right initial states are described as *numerically different* fluids, labeled + and −, even if of *physically identical* equations of state. As the present implementation of the scheme does not handle fluid disappearance—all fluids must be present in all cells, even if at low volume fractions,—the initial left and right states are asymmetric mixtures of the fluids with volume fractions $\alpha^{\pm}$ close but not equal to 0 and 1 as given in (67). In order to avoid physical mixing at the contact discontinuity, the fluid velocities were relaxed to a common value in each cell by momentum conservation at every time step: this implements a stick condition and can be interpreted as modifying the backbone model by either constraining the Lagrangian to a single velocity or by adding an infinitely strong drag force. No supplementary dissipation of kinetic energy is produced by this infinitely strong drag and the internal energy equations do not require any changes. In principle, sharp interfaces would be physically preserved when forcing equal velocities of the fluids, but they can still be smeared by numerical diffusion due to transport.

Results in Fig. 2 show that the symmetry of the problem is well preserved despite the large deformation of the cells. The scheme handles the shifting of Lagrangian and supersonic characteristics—black lines in maps of Fig. 2—without producing any numerical artifact nor oscillation. The impact of the grid motion is basically reduced to numerical diffusion, mostly visible by the smearing of the contact discontinuity between the two fluids as illustrated by the fluid volume fraction in Figs 2c and 2d. As expected, the slice of the mesh at $y \approx 0.2$, whose velocity exactly matches that of the contact discontinuity where transport fluxes cancel, shows negligible spreading of this singularity.

In order to reduce numerical diffusion at the contact discontinuity specific steepening or interface reconstruction algorithms could be introduced, but here the ALE capability of the scheme can also be exploited, for instance by simply prescribing the mesh displacement to depend on the near-Lagrangian velocity (66): i) nodes initially tagged at contact, $x = 1/2$, are moved according to the near-Lagrangian velocity, ii) nodes initially tagged at left and right boundaries, $x = 0$ or 1, are fixed, and iii) all other nodes move so as to be evenly distributed in-between these limits at all times. The ensuing results on density and volume fraction fields, illustrated in Fig. 3, show negligible spreading of the contact discontinuity and accurate capture of the three waves. It must be stressed that this was achieved without input of the otherwise available analytical solution of the Riemann problem, but by merely computing on-the-fly a near-Lagrangian velocity.

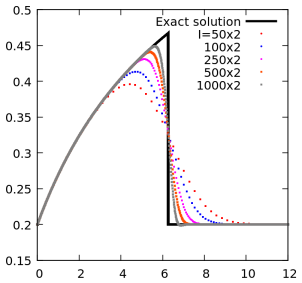

Figure 4: Volume fraction profiles for Ransom's water faucet problem computed with the present GEEC multi-fluid scheme. CFL = 0.8, 50×2 to 1000×2 cells, black line is exact solution.

6.3. *Ransom's faucet variant: two-dimensional, random grid*

Ransom's water faucet [117] is a 1D ideal two-fluid flow which is simply captured by the present two-fluid backbone model. It consists of a 12 m vertical pipe initially filled with a mixture of water and air at $P = 10^5$ Pa with uniform velocities and volume fractions $u^{\text{Water}} = 10$ m.s^{-1}, $u^{\text{Air}} = 0$, $\alpha^{\text{Water}} = 0.8$, and $\alpha^{\text{Air}} = 0.2$. Top boundary conditions are constant velocities and volume fractions $u^{\text{Water}} = 10$ m.s^{-1}, $u^{\text{Air}} = 0$, $\alpha^{\text{Water}} = 0.8$, and with $\alpha^{\text{Air}} = 0.2$. Bottom boundary conditions are free fluxes to ambient pressure $P = 10^5$ Pa. Equations of state for water and air are approximated by respectively stiffened and perfect gases as defined in Section 6.1 and no inter-fluid friction terms or any other dissipation effects are added (fluctuations, turbulence, pressure relation, etc.)—as sometimes done in order to stabilize elliptic modes at the expense of spurious distortions. Under the action of gravity $G = 10$ m.s^{-2}, the water initially in the pipe undergoes an undistorted "solid like" free fall—barely disturbed by the presence of air—while the constant flux stream flowing from the top accelerates and stretches. In the limit of incompressible water and infinite density ratio, an analytical solution is known [117] which provides an approximate but accurate enough reference for numerical results.

The two main features of the simulated flow are: i) the profile of the stretched stream, to be compared with the smooth analytical solution; and ii) the volume fraction discontinuity, to be captured without too much numerical diffusion or oscillations. They are usually examined on the gas volume fraction profile $\alpha^{\text{Air}}(t, x)$ at a fixed time, here $t = 0.5$. Two grid motion strategies are tested: i) a quasi-1D Eulerian grid, with fixed nodes $\boldsymbol{w} = \boldsymbol{0}$ in order to study the convergence of the solution; and ii) a 2D grid of square cells, dynamically distorted by a random-in-space-and-time field of node velocities $\boldsymbol{w}(t, \boldsymbol{x})$.

As shown in Fig. 4 for quasi-1D Eulerian grids from 50×2 to 1000×2 the scheme accurately captures the profile of the stretched stream while producing some diffusion of the volume fraction discontinuity. Despite transport being only first order,

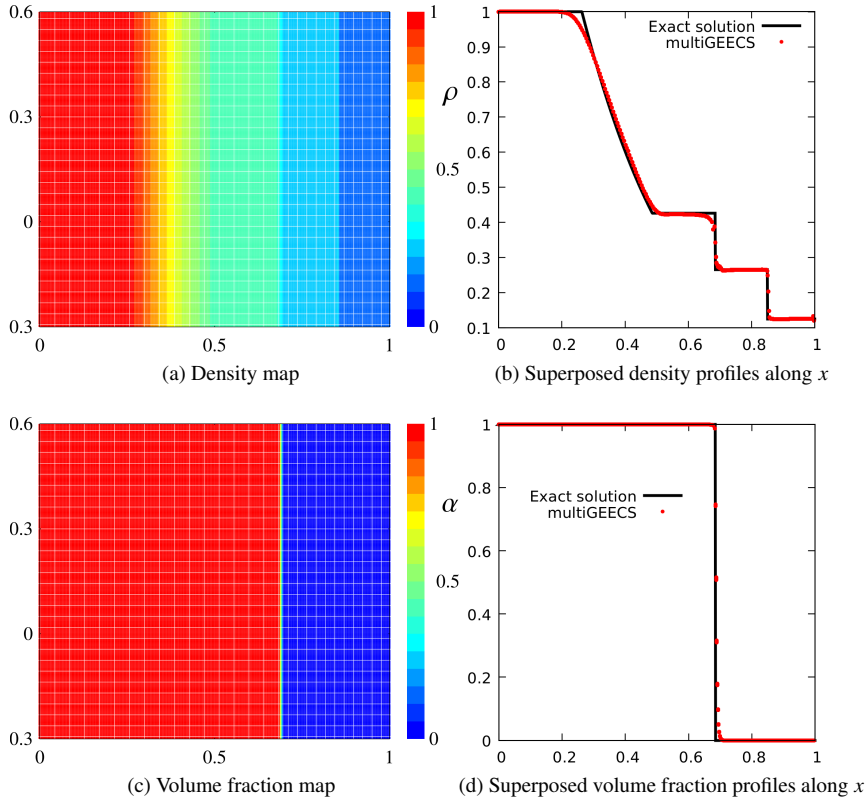

(a) Density map (b) Superposed density profiles along x

(c) Volume fraction map (d) Superposed volume fraction profiles along x

Figure 3: Density (top) and volume fraction (bottom) maps and profiles for the two-dimensional two-fluid Sod's shock tube computed with the present GEEC multi-fluid scheme on a grid linearly interpolated between the Lagrangian contact discontinuity and the side boundaries. CFL = 0.5, 320×290 cells, one in ten grid lines represented in both dimensions (white lines).

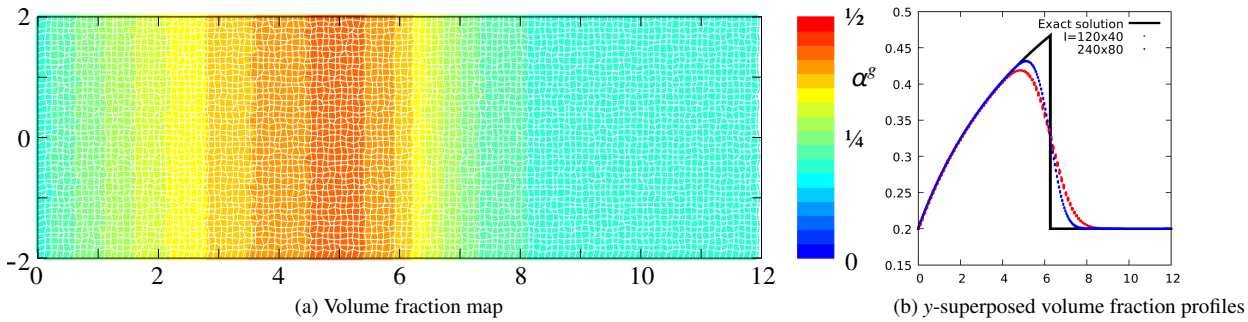

(a) Volume fraction map (b) y-superposed volume fraction profiles

Figure 5: Volume fraction map and profiles for Ransom's water faucet problem computed with the present GEEC multi-fluid scheme on a randomly distorted ALE grid. CFL = 0.8, 120×40 cells (left), 120×40 and 240×80 cells (right), black line is exact solution.

these results compare very favorably with previous results obtained with other schemes on the same six-equation backbone model [28]: as previously noted [28], the thermodynamic consistency of the scheme is one of the crucial elements to robustly capture the here quasi-isentropic behavior of the fluids. Robustness is estimated by the highest CFL value before code "crash," here found to be above the high value of 0.8.

For the finest mesh, a slight undershoot appears in the volume fraction profiles upstream of the discontinuity which is generally recognized to be a consequence of the non hyperbolic behavior of the two-fluid backbone model—a form of Kelvin–Helmholtz instability [36, § IV]. As already discussed [see for instance 28, and references therein], the amplification of this physical oscillation is always present, even if not visible at early times, and occurs sooner when numerical dissipation is reduced through mesh refinement.

Figure 5a displays the volume fraction map for Ransom's water faucet problem performed on a randomly distorting mesh. The $[0; 12]\times[0; 4]$ domain is initially meshed with 120×40 uniform square cells which are then dynamically distorted by a grid velocity defined by $\boldsymbol{w} = (w_x, w_y)$ where w_x and w_y are random numbers drawn between $\pm10^{-2}$ at each time step. Figure 5b displays the superposed volume fraction profiles for two mesh sizes 120×40 and 240×80. Even with a relatively coarse grid

submitted to random motions, the position and level of the volume fraction discontinuity are properly captured. The amount of numerical diffusion can be reduced by increasing the number of mesh cells.

6.4. Supersonic crossing of eight Gaussian clouds on shrink-then-stretch swirling ALE grid

Many elementary test cases for multi-fluid flows are available in the literature on which the present scheme could or has been [42, § 4.5] applied. However, its combined features deserve being tested on a specific and demanding configuration. The present "supersonic crossing of eight Gaussian clouds" aims at simultaneously stressing the discretized pressure work terms by as many effects as possible: i) highly contrasted equations of state, here water and air, ii) large and extreme changes in volume fraction, down to the percent range in air, iii) supersonic drift velocities with respect to air's speed of sound, subsonic and supersonic with respect to water's, and iv) large transport with respect to an ALE grid undergoing large distortions including volume changes.

This 2D test involves eight packets or clouds of water in a background of still air. The clouds and the background are each represented by separate fluids thus defining a nine-fluid system whose evolution can thus be captured by the present scheme. Though described by separate equations, the eight water clouds have the same equation of state provided in Section 6.1. Apart of pressure terms, no interactions between the clouds or between clouds and air are added—collisions, drag, thermal transfers, etc. *Clouds can thus cross each other freely*. The computation domain is $[-3;3]\times[-3;3]$ m. The initial condition at $t=0$ consists in cloud volume fractions $\alpha^\varphi(0,\boldsymbol{x})$, all with Gaussian profiles of amplitudes 0.15 and root mean square radii 0.2 m, but centered at different positions $\boldsymbol{x}_0^\varphi$ and set in different uniform motions $\boldsymbol{u}^\varphi(0,\boldsymbol{x})=\boldsymbol{u}_0^\varphi$ according to

φ	x_0^φ (m)	y_0^φ (m)	u_{0x}^φ (m.s^{-1})	u_{0y}^φ (m.s^{-1})
1, 2	±1	0	∓1000	0
3, 4	0	±1	0	∓1000
5, 6	±2	0	∓2000	0
7, 8	0	±2	0	∓2000

(68)

(notice matched ± and ∓ signs). The velocity field of the air background is initially set so that the mean volume weighted velocity cancels, $\overline{\boldsymbol{u}}=\sum_\varphi \alpha^\varphi\boldsymbol{u}^\varphi=\boldsymbol{0}$. Boundary conditions are perfect zero flux walls. The computation is carried out up to time $t=2\times10^{-3}$ s on an initially-Cartesian shrink-then-stretch swirling ALE grid defined by a node velocity field given as

$$w_x(t,x,y)=[\sigma x/L+\cos(\pi x/L)\sin(\pi y/L)]\times L/\tau\,, \tag{69a}$$

$$w_y(t,x,y)=[\sigma y/L-\cos(\pi y/L)\sin(\pi x/L)]\times L/\tau\,, \tag{69b}$$

$$\tfrac{\mathrm{d}}{\mathrm{d}t}L(t)=\sigma L/\tau\,. \tag{69c}$$

with $L(0)=3$ m, $\tau=2\times10^{-3}$ s, and $\sigma=-1$ or $+1$ for respectively $t<\tau/2$ or $>\tau/2$. The grid is thus shrunk to about 60% at $t=10^{-3}$ s and swirled at the center by about a half turn at final time.

Figure 6 displays the volume fraction maps produced at $t=0$, 10^{-3}, and 2×10^{-3} s by the present GEEC multi-fluid scheme for the eight Gaussian clouds crossing on a 480×480 mesh. At $t=10^{-3}$ s, all the clouds cross (without merging) at the origin where the air volume fraction drops to $\alpha^{\mathrm{Air}}\approx3.8\%$. At final time $t=2\times10^{-3}$ s, the clouds occupy opposite positions with respect to the initial configuration, their trajectory being marginally affected by the crossing and by the air motion despite the large volume fraction variations and the severe mesh distortion. The only visible distortion of the clouds is the expected smearing due to numerical diffusion. An animated version of this test is provided as supporting information on the journal's web site.

This test is akin to collisions of particle jets, often simulated by Euler–Lagrange approaches as in Ref. [118, § 4.3], which are important benchmarks of schemes used in spray simulations.

7. Conclusion

The present work provides a consistent and robust discretization of the compressible multi-fluid backbone model, which ensures geometric, energetic, and entropic compatibility in a direct ALE setting. It was successfully tested on various ideal but constraining 2D flow configurations thus showing its potential for further enrichment with dissipation terms such as viscosity, drag, thermal transfers, etc. for simulating a wide range of practical configurations.

In its present version, the general features of the scheme are: i) arbitrary number of fluids; ii) arbitrary mesh dimension, structure, and motion—prescribed by the user or adjusted on-the-fly to the flow's evolution;—iii) continuity with the workhorse space-and-time-staggered schemes of in-house legacy codes; iv) explicit mass, momentum, and internal energy increment equations for each fluid, coupled by a single common pressure field; v) exact conservation to round-off errors of each fluid's mass, total momentum, and total energy; vi) second-order accuracy in the Lagrangian limit and first-order accuracy of fluid transport relative to the grid; vii) proper capture to second-order accuracy of isentropic flows—or quasi-symplectic behavior;—viii) shock capture and scheme stabilization ensured by a proper multi-fluid extension of usual single-fluid closures of artificial viscosity; and viii) stable and robust behavior with high CFL condition on usual stiff test cases—devoid of common distortions such as hourglassing, De-Bar artifacts, fragility to small volume fractions or large density ratios, etc.

These properties were obtained by extending a three-step procedure already introduced [64, 67] when revisiting the historical scheme of von Neumann and Richtmyer [62], and now designated as GEEC for "Geometry, Energy, and Entropy Compatible [43]." It consists in: i) applying a discrete least action variational principle—which mimics the derivation of the continuous evolution equations from kinetic and internal energies—to build the proper isentropic momentum equations in the present multi-fluid ALE setting; ii) enforcing energy conservation and consistency with fundamental thermodynamic re-

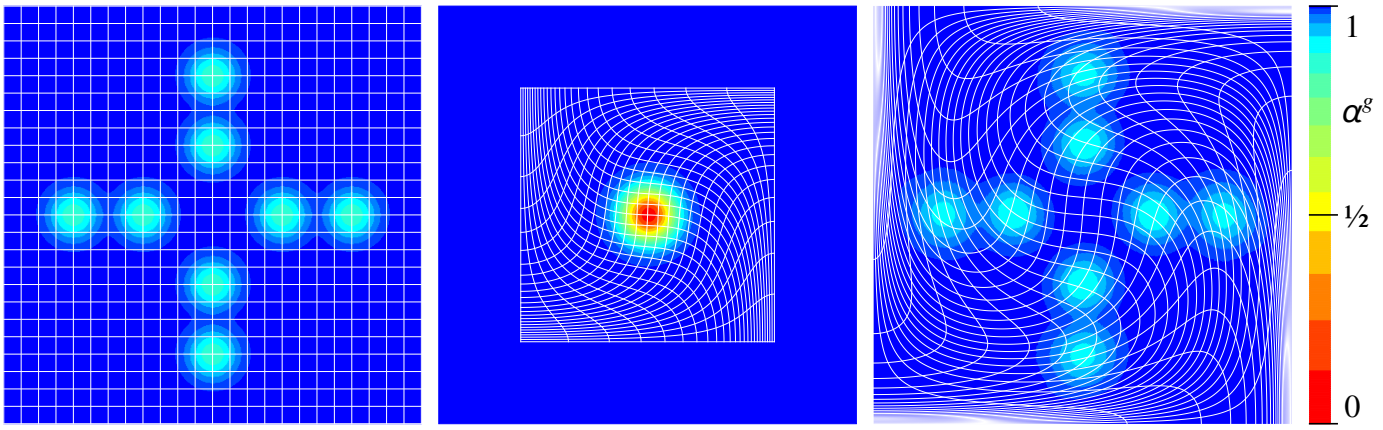

Figure 6: Volume fraction maps at times $t = 0$ (left), $t = 10^{-3}$ (center), and $t = 2 \times 10^{-3}$ s (right, final) for the nine-fluids crossing test on a shrink-then-stretch swirling grid. Residual volume fraction of air at center at $t = 10^{-3}$ s is $\alpha^{\text{Air}} \approx 3.8\%$. CFL = 0.7, 480×480 cells, one in twenty grid lines represented in both dimensions (white lines). An animated version is provided as supporting information on the journal's web site.

lations to produce explicit energy equations; and iii) adding dissipative processes to the equations, for instance for shock capture.

In the course of the derivation, the proper isentropic behavior constrained the scheme with two non-trivial features: i) the discrete pressure gradient operator must be an adapted *downwind* dual of the *upwind* transport operators—as already observed in the single-fluid case [43, § 2.6];—and ii) the internal energy equations must be made *explicit* and *decoupled* from other equations by separating the various physical and numerical contributions to pressure work. The pressure downwinding derivation confirms and justifies previous observations showing that the low Mach behavior of single-fluid schemes is improved by pressure gradient centering [109, § 5.3] or by the implicit downwinding embedded in Lagrange-plus-Remap approaches [110–112]. Explicit equations for internal energies yield simpler and uncoupled calls to the equations of state and also provide a stiffness analysis of all the pressure work effects.

The GEEC approach embodies two principles of hydroschemes which have been recently put forward. Quoting for instance P. Roe [119, § 10]: "There should be no dissipation if no dissipation is needed. There should be distinctly different approaches to the propagation of advective and acoustic disturbances, because in more than one dimension there is little that these phenomena have in common." The present variational procedure is built upon a minimal dissipation and an upfront separation of advective and pressure fluxes.

With added dissipation terms—drag, collisions, thermal transfers, etc.—this scheme can meet the requirements of multi-fluid simulations in many applications. Yet, it appears more valuable as a general *proof of concept* of variational mimicking approaches applied to multi-fluid scheme design. Extensions to full second-order accuracy and to other non-dissipative effects—inter-particle pressure or turbulence, added mass, surface tension, etc.—are straightforward in principle. The ensuing technicalities and tediousness of such derivations may appear intractable by hand but would be accessible to symbolic calculation software with automated source code generation. Efforts are being pursued along these lines.

Acknowledgments

We are very grateful towards Éric Heulhard de Montigny and Christina Paulin for carefully testing and correcting the scheme.

Appendix A. On ellipticity as defined by eigenmodes

The present appendix provides an expanded and more rigorous version of the discussion in Section 1.2 following the very widespread approach of plane-wave perturbations (or von Neumann stability analysis) which has been applied to multi-fluid systems in different contexts and variations for over forty years. A discussion on the subtle relation between this and other approaches can be found in Ref. [36].

Consider a generic system for two- or multi-fluid equations of formal type

$$\partial_t \boldsymbol{U} + \boldsymbol{B}_1(\boldsymbol{\nabla} \otimes \boldsymbol{U}) = \boldsymbol{D}_0(\boldsymbol{U}) + \boldsymbol{D}_1(\boldsymbol{\nabla} \otimes \boldsymbol{U}) + \boldsymbol{D}_2(\boldsymbol{\nabla} \otimes \boldsymbol{\nabla} \otimes \boldsymbol{U}) \,, \quad \text{(A.1)}$$

where $\boldsymbol{U}(t, \boldsymbol{x})$ is the vector field of the fluids' conservative quantities (densities, momenta and total energies), $\boldsymbol{B}_1$ is the (backbone) non-dissipative operator, and $\boldsymbol{D}_0$, $\boldsymbol{D}_1$, and $\boldsymbol{D}_2$ are the other mostly dissipative terms which operate on space derivatives of respective ranks 0, 1, and 2. In order to preserve homogeneity with the time derivative $\partial_t \boldsymbol{U}$, these operators must involve characteristic factors scaling as *frequencies* $\sim 1/T$, *velocities* $\sim L/T$, and *diffusion coefficients* $\sim L^2/T$ according to their respective ranks 0, 1, and 2. Other terms can also be considered but do not change in essence the discussion to follow. Characteristic velocities in $\boldsymbol{B}_1$ are built from combinations of fluid velocities and speeds of sound as visible in the non-dissipative terms investigated in the present work.

Formally expanding (A.1) to first order into a plane-wave perturbation of frequency $\omega_{\boldsymbol{k}}$ and wave vector $\boldsymbol{k}$ around a stationary and uniform solution, $\boldsymbol{U} = \boldsymbol{U}_0 + \boldsymbol{u}_{\boldsymbol{k}} \exp[i(\omega_{\boldsymbol{k}} t - \boldsymbol{k} \cdot \boldsymbol{x})]$,

yields the linear system in $\boldsymbol{u_k}$

$$\begin{aligned} &i\omega_{\boldsymbol{k}}\boldsymbol{u_k} - i\boldsymbol{k}\cdot\tfrac{\partial \boldsymbol{B}_1}{\partial(\boldsymbol{\nabla}\otimes\boldsymbol{U})}\cdot\boldsymbol{u_k} \\ &= \tfrac{\partial \boldsymbol{D}_0}{\partial \boldsymbol{U}}\cdot\boldsymbol{u_k} - i\boldsymbol{k}\cdot\tfrac{\partial \boldsymbol{D}_1}{\partial(\boldsymbol{\nabla}\otimes\boldsymbol{U})}\cdot\boldsymbol{u_k} - (\boldsymbol{k}\otimes\boldsymbol{k}) : \tfrac{\partial \boldsymbol{D}_2}{\partial(\boldsymbol{\nabla}\otimes\boldsymbol{\nabla}\otimes\boldsymbol{U})}\cdot\boldsymbol{u_k}\,. \end{aligned} \tag{A.2}$$

$\omega_{\boldsymbol{k}}$ and $\boldsymbol{u_k}$ are thus the eigenvalue and eigenvector of a linear operator that combines the non-dissipative and dissipative contributions *scaled by powers of* $\boldsymbol{k}$. Depending on the presence, magnitude, spectra, and degeneracy of these contributions, various situations can appear, of which four limiting cases are of special interest here

$\boldsymbol{D}_0 = \boldsymbol{D}_1 = \boldsymbol{D}_2 = \boldsymbol{0}$, dissipation free: $\omega_{\boldsymbol{k}} \propto \boldsymbol{k}$

$$\omega_{\boldsymbol{k}}\boldsymbol{u_k} = \boldsymbol{k}\cdot\tfrac{\partial \boldsymbol{B}_1}{\partial(\boldsymbol{\nabla}\otimes\boldsymbol{U})}\cdot\boldsymbol{u_k}\,, \tag{A.3a}$$

$\boldsymbol{D}_0 \neq \boldsymbol{0}$, $\boldsymbol{k}\to\boldsymbol{0}$, drag-like dissipation: $\omega_{\boldsymbol{k}} \propto \boldsymbol{k}^0$

$$\omega_{\boldsymbol{k}}\boldsymbol{u_k} = -i\tfrac{\partial \boldsymbol{D}_0}{\partial \boldsymbol{U}}\cdot\boldsymbol{u_k}\,, \tag{A.3b}$$

$\boldsymbol{D}_0 = \boldsymbol{D}_2 = 0$, "flat dissipation:" $\omega_{\boldsymbol{k}} \propto \boldsymbol{k}$

$$\omega_{\boldsymbol{k}}\boldsymbol{u_k} = \boldsymbol{k}\cdot\left(\tfrac{\partial \boldsymbol{B}_1}{\partial(\boldsymbol{\nabla}\otimes\boldsymbol{U})} - \tfrac{\partial \boldsymbol{D}_1}{\partial(\boldsymbol{\nabla}\otimes\boldsymbol{U})}\right)\cdot\boldsymbol{u_k}\,, \tag{A.3c}$$

$\boldsymbol{D}_2 \neq \boldsymbol{0}$, $\|\boldsymbol{k}\|\to\infty$, diffusion-like dissipation: $\omega_{\boldsymbol{k}} \propto \boldsymbol{k}^2$

$$\omega_{\boldsymbol{k}}\boldsymbol{u_k} = i(\boldsymbol{k}\otimes\boldsymbol{k}) : \tfrac{\partial \boldsymbol{D}_2}{\partial(\boldsymbol{\nabla}\otimes\boldsymbol{\nabla}\otimes\boldsymbol{U})}\cdot\boldsymbol{u_k}\,. \tag{A.3d}$$

Case (A.3a) is the (elliptic) backbone model whose operator spectrum, as is well known, contains conjugate complex eigenvalues proportional to $\boldsymbol{k}$. Because of the imaginary factor i in the wave phase, this produces discontinuous sensitivity to initial conditions as perturbations at divergingly large $\boldsymbol{k}$ (or small scales) experience exponential growth at divergingly fast rate $\omega_{\boldsymbol{k}}$.

Case (A.3b) is produced for instance when adding drag to the backbone model, with generally *negative* eigenvalues. Thus, below a cutoff wavevector of magnitude $\sim \|\tfrac{\partial \boldsymbol{D}_0}{\partial \boldsymbol{U}}\|/\|\tfrac{\partial \boldsymbol{B}_1}{\partial(\boldsymbol{\nabla}\otimes\boldsymbol{U})}\|$ it may relax perturbations in finite time, but cannot damp the divergingly fast instabilities at divergingly large $\boldsymbol{k}$ of case (A.3a).

Case (A.3c) is produced for instance by various stabilization techniques such as artificial drag [120, 121, eq. 15 & § 3], added mass [76, 122, § 6], or supplementary evolution equations for pressure relation [15]. No cutoff wavelength appears and careful crafting of $\boldsymbol{D}_1$ may achieve damping of instabilities for all values of $\boldsymbol{k}$. It is however unlikely that an actual physical process may be able to *exactly* compensate the instability of the backbone model across the *whole range* of $\boldsymbol{k}$.

Case (A.3d) is produced for instance when adding diffusion, viscosity, or conduction, with generally *positive* eigenvalues. Thus, above a cutoff wave vector of magnitude $\sim \|\tfrac{\partial \boldsymbol{B}_1}{\partial(\boldsymbol{\nabla}\otimes\boldsymbol{U})}\|/\|\tfrac{\partial \boldsymbol{D}_2}{\partial(\boldsymbol{\nabla}\otimes\boldsymbol{\nabla}\otimes\boldsymbol{U})}\|$ it may relax in finite time the otherwise divergingly fast instabilities at divergingly large $\boldsymbol{k}$ of case (A.3a). This weak stabilization is always present in calculations because of *numerical* dissipation at cell-size cutoff $1/h$. Some physical situations require that low $\boldsymbol{k}$ modes remain unstable as representing Kelvin–Helmoltz like instabilities [36, § IV] which are of prime importance as seeds for slug flows [123].

These situations and other combinations have been studied for instance in Ref. [40]. An interesting alternative to the strong stabilization provided by case (A.3c), "ideal" but often unphysical, is the combination of the long and short wavelength damping of cases (A.3b) and (A.3d): this requires closing the gap of possible unstable modes, thus yielding a condition of type $\|\tfrac{\partial \boldsymbol{B}_1}{\partial(\boldsymbol{\nabla}\otimes\boldsymbol{U})}\|^2 \lesssim \|\tfrac{\partial \boldsymbol{D}_0}{\partial \boldsymbol{U}}\| \times \|\tfrac{\partial \boldsymbol{D}_2}{\partial(\boldsymbol{\nabla}\otimes\boldsymbol{\nabla}\otimes\boldsymbol{U})}\|$ [see for instance 124, Appendix].

The above comments summarize findings by numerous (early and notable) investigators of multi-fluid flows, some of which are deservedly quoted below.

[34, § 6.4, translated from French by the authors]: "The presence of differential terms in the transfer laws [between fluids] turns out to be an essential characteristic of the system. They must be taken into account in modeling."

[35, § 'Stability']: "[...] the ill-posed nature is precluded by dissipative processes, which are especially effective in damping the highest frequency components of any perturbation, at the same time having relatively little effect on the larger scale fluctuations."

[36, § VI]: "[...] the single most essential modification to the basic equation system is the introduction of such short-wavelength effects as surface tension or viscosity. In retrospect, this modification is clearly suggested by the well-known fact that such effects are sufficient to stabilize short wavelengths and produce properly posed problems in other contexts."

[37, § 'Conclusions']: "[...] numerical calculation with a two-fluid finite-difference model of two-phase flow can be well-behaved provided there is sufficient momentum transfer between phases, and the spatial mesh is not too fine."

[38, § 3]: "[...] the indicated systems of equations correctly define the behavior of a disperse mixture only when the characteristic distances considered in the problem (in particular the wave length λ) are considerably greater than the dispersed particle dimension a. It is, therefore possible to assume that the boundless increase of the exponent of $-D$ as $\lambda \to 0$ is the consequence of the neglect in equations of type (1.1) or (3.1) of some dissipation processes that occur when ultrashort waves $\lambda \lesssim a$ pass through disperse media."

[32, § 2.3]: "With the inclusion of any nonzero viscosity, no matter how small, the basic model becomes well-posed in the sense that for the linearized frozen coefficient problem, perturbations of wave number k are bounded as $k \to \infty$, for any fixed time [...] Thus, it seems improper to consider the behavior of the differential equations at arbitrarily small wavelengths without including viscosity, which is not zero for real fluids and gases."

[39, § 6]: "[...] the flow instabilities present in the mean motion equations of two-phase flow can be explained as a result of the failure to include appropriate closure models for the velocity fluctuations in the momentum equations. If these terms are neglected unstable mean flow equations are exactly what one should expect and what one obtains."

[33, § 6]: "The degree of ill-posedness is therefore defined by the role and effect of the lost, filtered-out, sub-grid-scale information on the collective, global flow behavior described by the averaged field equations."

Appendix B. Notations, definitions

Labels, indices:

φ, ϕ	fluid labels, with $1 \leq \varphi, \phi \leq \Phi$.
i, j	= 1, 2, 3, or x, y, z, coordinate labels.
n, $n+1/2$	time labels.
c, d	cell labels.
p	node label.
$\mathcal{C}(p)$	set of cell labels around node p.

Continuous and discrete coordinates and geometry:

h, h_c^n	typical size of cell, or of cell c at time n.
t, t^n, $t^{n+1/2}$	time values, generic and discrete, with $t^{n+1/2} = (t^n + t^{n+1})/2$.
Δt^n, $\Delta t^{n+1/2}$	integer and half-integer time steps.
$\boldsymbol{x}$, $\boldsymbol{x}_p^n$	position, generic and of node p at time t^n.
V_c^n	volume of cell c at time n (unrelated to $\mathring{V}_{cd}^{\varphi n+1/2}$).
$\boldsymbol{s}_{cd}^n$	outward pointing vector normal to boundary element from cell c to cell d at time n (amplitude given by area of boundary element, $\boldsymbol{s}_{cd}^n = -\boldsymbol{s}_{dc}^n$).

Continuous and discrete fields (respectively functions of t and $\boldsymbol{x}$, or indexed by n or $n+1/2$, and c or p):

ρ^φ, $\rho_c^{\varphi n}$	mass density of fluid φ.
e^φ, $e_c^{\varphi n}$	per-mass internal energy of fluid φ.
c^φ, $c_c^{\varphi n}$	speed of sound in fluid φ.
c, c_c^n	effective zero-drag adiabatic speed of sound of fluid mixture.
P, P_c^n	common pressure of fluids.
Q, Q_c^n	total artificial viscosity stress.
Q^φ, $Q_c^{\varphi n}$	artificial viscosity stress in fluid φ.
$\mathring{W}^\varphi$, $\mathring{W}_c^{\varphi n+1/2}$	irreversible energy production on fluid φ.
$\boldsymbol{w}$, $\boldsymbol{w}_p^{n+1/2}$, $\boldsymbol{w}_c^{n+1/2}$	grid velocity.
$\boldsymbol{v}^\varphi$, $\boldsymbol{v}_c^{\varphi n+1/2}$	relative-to-grid velocity of fluid φ.
$\boldsymbol{u}^\varphi$, $\boldsymbol{u}_c^{\varphi n+1/2}$	$= \boldsymbol{w}_c^{n+1/2} + \boldsymbol{v}_c^{\varphi n+1/2}$, absolute velocity of fluid φ.
$\overline{\boldsymbol{u}}$	$= \sum_\varphi \alpha^\varphi \boldsymbol{u}^\varphi$, volume averaged absolute velocity.
$\mathring{V}_{cd}^{\varphi n+1/2}$	$= \sigma_{cd}^{\varphi n+1/2} \boldsymbol{s}_{cd}^{n+1/2} \cdot \boldsymbol{v}_c^{\varphi n+1/2}$, volume transport rate of fluid φ from cell c to cell d at time $n+1/2$.
$\sigma_{cd}^{\varphi n+1/2}$	$= H(\boldsymbol{s}_{cd}^{n+1/2} \cdot \boldsymbol{v}_c^{\varphi n+1/2})$, transport upwind factor of fluid φ from cell c to cell d at time $n+1/2$.
$\overline{\sigma}_{cd}^{\varphi n+1/2}$	corrected upwinding factor of fluid φ from cell c to cell d at time $n+1/2$.
α^φ, $\alpha_c^{\varphi n}$	volume fraction of fluid φ.
$[\alpha\rho]^\varphi$, $[\alpha\rho]_c^{\varphi n}$	$= \alpha_c^{\varphi n} \rho_c^{\varphi n}$, mass per-total-volume of fluid φ.
β^φ, $\beta_c^{\varphi n}$	global compressibility weighting coefficient of fluid φ.
γ^φ, $\gamma_c^{\varphi n}$	adiabatic exponent of fluid φ.
Γ^φ, $\Gamma_c^{\varphi n}$	Grüneisen coefficient of fluid φ.
λ^φ, $\lambda_c^{\varphi n}$	global dissipation weighting coefficient of fluid φ (impacts artificial dissipation).
$\mu^{\varphi\phi}$, $\mu_c^{\varphi\phi n}$	relative compressibility weighting coefficient between fluids φ and ϕ.
π^φ, $\pi_c^{\varphi n}$	pressure offset for stiffened gas equation of state of fluid φ.
ϕ^φ, $\phi_c^{\varphi n}$	Lagrange multiplier of mass transport of fluid φ.
ψ^φ, $\psi_c^{\varphi n}$	Lagrange multiplier of Lagrangian coordinate transport of fluid φ.
ξ^φ, $\xi_c^{\varphi n}$	Lagrangian coordinate field of fluid φ.
Π, Π_c^n	Lagrange multiplier of volume fraction closure.

Miscellaneous:

D_t^φ, $\mathrm{D}_{\Delta t}^\varphi$	"Eulerian" transport derivative along velocity of fluid φ, continuous and discrete.
d_t^φ, $\mathrm{d}_{\Delta t}^\varphi$	"Lagrangian" transport derivative along velocity of fluid φ, continuous and discrete.
$\mathcal{A}$	continuous or discrete action integral.
$\mathcal{L}$	continuous Lagrangian density.
$\mathcal{P}^\varphi$	pressure function as given by equation of state of fluid φ.
$\mathcal{Q}$	normalized artificial viscosity function.
δ	variation operator.
$\langle \boldsymbol{u}^\varphi \cdot \boldsymbol{\nabla} P \rangle_c^n$	power of pressure forces on fluid φ.
$\langle \mathring{V} \rangle_c^n$	mean volume derivative of fluid mixture.
$\langle \rho^\varphi \, \delta W^\varphi \rangle_c^n$	irreversible energy production on fluid φ.

References

[1] O. J. Nydal, Dynamic models in multiphase flow, Energy Fuels 26 (7) (2012) 4117–4123. doi:10.1021/ef300282c.

[2] M. Shippen, W. J. Bailey, Steady-state multiphase flow – past, present, and future, with a perspective on flow assurance, Energy Fuels 26 (7) (2012) 4145–4157. doi:10.1021/ef300301s.

[3] K. Havre, K. O. Stornes, H. Stray, Taming slug flow in pipelines, ABB Rev 2000 (4) (2000) 55–63.
URL https://search-ext.abb.com/library/Download.aspx?DocumentID=100580A1337&Action=Launch

[4] A. S. Shieh, V. H. Ransom, R. Krishnamurthy, RELAP5/MOD3 code manual Vol. 6. Validation of numerical techniques in RELAP5/MOD3, Tech. Rep. Report NUREG/CR-5535, Idaho National Engineering Laboratory (1994).

[5] US Nuclear Regulatory Commission, TRACE V5.0; Theory manual; User's manual volume 1: Input specification, volume 2: modeling guidelines; Assessment manual (2008).

[6] S. H. Ahn, N. Aksan, H. Austregesilo, D. Bestion, B. D. Chung, F. D'Auria, P. Emonot, J. L. Gandrille, M. Hanninen, I. Horvatović, K. D. Kim, A. Kovtonyuk, A. Petruzzi, FONESYS: the FOrum & NEtwork of SYStem thermal-hydraulic codes in nuclear reactor thermal-hydraulics, Nucl Eng Des 281 (2015) 103–113. doi:10.1016/j.nucengdes.2014.12.001.

[7] C. E. Brennen, Cavitation and bubble dynamics, Oxford, 1995.
URL https://authors.library.caltech.edu/25017/1/cavbubdynam.pdf

[8] S. Jay, F. Lacas, S. Candel, Combined surface density concepts for dense spray combustion, Combust Flame 144 (3) (2006) 558–577. doi:10.1016/j.combustflame.2005.07.017.

[9] M. J. Sapko, E. S. Weiss, K. L. Cashdollar, I. A. Zlochower, Experimental mine and laboratory dust explosion research at NIOSH, J Loss Prev Process Ind 13 (3–5) (2000) 229–242. doi:10.1016/S0950-4230(99)00038-8.

[10] Y. P. Zheng, C. G. Feng, G. X. Jing, X. M. Qian, X. J. Li, Z. Y. Liu, P. Huang, A statistical analysis of coal mine accidents caused by coal dust explosions in China, J Loss Prev Process Ind 22 (4) (2009) 528–532. doi:10.1016/j.jlp.2009.02.010.

[11] N. G. Deen, M. Van Sint Annaland, M. A. Van der Hoef, J. A. M. Kuipers, Review of discrete particle modeling of fluidized beds, Chem Eng Sci 62 (1) (2007) 28–44. doi:10.1016/j.ces.2006.08.014.

[12] L. Wilson, Relationships between pressure, volatile content and ejecta velocity in three types of volcanic explosion, J Volcanol Geotherm Res 8 (2) (1980) 297–313. doi:10.1016/0377-0273(80)90110-9.

[13] A. Murrone, P. Villedieu, Numerical modeling of dispersed two-phase flows, AerospaceLab 2 (4) (2011) 1–13.
URL https://www.aerospacelab-journal.org/sites/www.aerospacelab-journal.org/files/AL2-04.pdf

[14] A. Vallet, R. Borghi, An Eulerian model of atomization of a liquid jet, C R Acad Sci, Ser IIb: Mec, Phys, Chim, Astron 327 (10) (1999) 1015–1020. doi:10.1016/S1287-4620(00)87013-1.

[15] M. R. Baer, J. W. Nunziato, A two-phase mixture theory for the Deflagration-to-Detonation Transition (DDT) in reactive granular materials, Int J Multiphase Flow 12 (6) (1986) 861–889. doi:10.1016/0301-9322(86)90033-9.

[16] A. Chinnayya, E. Daniel, R. Saurel, Modelling detonation waves in heterogeneous energetic materials, J Comput Phys 196 (2) (2004) 490–538. doi:10.1016/j.jcp.2003.11.015.

[17] M. Brennan, CFD simulations of hydrocyclones with an air core: comparison between large eddy simulations and a second moment closure, Chem Eng Res Des 84 (6) (2006) 495–505. doi:10.1205/cherd.05111.

[18] A. Davailles, E. Climent, F. Bourgeois, Fundamental understanding of swirling flow pattern in hydrocyclones, Sep Purif Technol 92 (2012) 152–160. doi:10.1016/j.seppur.2011.12.011.

[19] M. Narasimha, M. Brennan, P. N. Holtham, A review of CFD modelling for performance predictions of hydrocyclone, Eng Appl Comput Fluid Mech 1 (2) (2007) 109–125. doi:10.1080/19942060.2007.11015186.

[20] V. J. Chanteperdrix, P. Villedieu, J.-P. Vila, A compressible model for separated two-phase flows computations, Vol. 1 of ASME Fluids Engineering Division Summer Meeting, 2002, pp. 809–816. doi:10.1115/FEDSM2002-31141.

[21] J.-M. Delhaye, Équations fondamentales des écoulements diphasiques, première partie : Équations générales de conservation, Tech. Rep. CEA-R-3429, Commissariat à l'Énergie Atomique (1968).
URL http://www.iaea.org/inis/collection/NCLCollectionStore/_Public/35/094/35094936.pdf?r=1

[22] D. A. Drew, Averaged field equations for two-phase media, Stud Appl Math 50 (2) (1971) 133–166. doi:10.1002/sapm1971502133.

[23] M. Ishii, T. Ibiki, Thermo-fluid dynamic theory of two-phase flow, Springer, 2011. doi:10.1007/978-1-4419-7985-8.

[24] C. E. Brennen, Fundamentals of multiphase flows, Cambridge, 2005.
URL https://authors.library.caltech.edu/25021/2/cabook.pdf

[25] A. Llor, Statistical hydrodynamic models for developed mixing instabilities flows: analytical 0D evaluation criteria, and comparison of single- and two-phase flow approaches, Vol. 681 of Lect Notes Phys, Springer, 2005. doi:10.1007/11531746.

[26] E. E. Michaelides, C. T. Crowe, J. D. Schwarzkopf (Eds.), Multiphase flow handbook, Taylor & Francis, CRC Press, 2016. doi:10.1201/9781315371924.

[27] M. López de Bertodano, W. Fullmer, A. Clausse, V. H. Ransom, Two-fluid model stability, simulation and chaos, Springer, 2017. doi:10.1007/978-3-319-44968-5.

[28] T. Vazquez-Gonzalez, A. Llor, C. Fochesato, Ransom test results from various two-fluid schemes: is enforcing hyperbolicity a thermodynamically consistent option?, Int J Multiphase Flow 81 (2016) 104–112. doi:10.1016/j.ijmultiphaseflow.2015.12.007.

[29] R. Saurel, R. Abgrall, A multiphase Godunov method for compressible multifluid and multiphase flows, J Comput Phys 150 (2) (1999) 425–467. doi:10.1006/jcph.1999.6187.

[30] R. Saurel, O. Le Metayer, A multiphase model for compressible flows with interfaces, shocks, detonation waves and cavitation, J Fluid Mech 431 (2000) 239–271. doi:10.1017/S0022112000003098.

[31] C. H. Chang, M. S. Liou, A robust and accurate approach to computing compressible multiphase flow: stratified flow model and AUSM$^+$-up scheme, J Comput Phys 225 (1) (2007) 840–873. doi:10.1016/j.jcp.2007.01.007.

[32] H. B. Stewart, B. Wendroff, Two-phase flow: models and methods, J Comput Phys 56 (3) (1984) 363–409. doi:10.1016/0021-9991(84)90103-7.

[33] T. N. Dinh, R. R. Nourgaliev, T. G. Theofanous, Understanding the ill-posed two-fluid model, in: 10th International Topical Meeting on Nuclear Reactor Thermal Hydraulics (NURETH-10), Seoul, Korea, 2003.
URL https://citeseerx.ist.psu.edu/viewdoc/summary?doi=10.1.1.517.5412

[34] J. Bouré, Dynamique des ecoulements diphasiques: propagation de petites perturbations, Tech. Rep. CEA-R-4466, Commissariat à l'Énergie Atomique (1973).
URL https://inis.iaea.org/collection/NCLCollectionStore/_Public/06/187/6187613.pdf

[35] J. R. Travis, F. H. Harlow, A. A. Amsden, Numerical calculation of two-phase flows, Nucl Sci Eng 61 (1) (1976) 1–10. doi:10.13182/NSE76-A28455.

[36] J. D. Ramshaw, J. A. Trapp, Characteristics, stability, and short-wavelength phenomena in two-phase flow equation systems, Nucl Sci Eng 66 (1) (1978) 93–102. doi:10.13182/NSE78-A15191.

[37] H. B. Stewart, Stability of two-phase flow calculation using two-fluid models, J Comput Phys 33 (2) (1979) 259–270. doi:10.1016/0021-9991(79)90020-2.

[38] L. A. Klebanov, A. E. Kroshilin, B. I. Nigmatulin, R. I. Nigmatulin, On the hyperbolicity, stability and correctness of the Cauchy problem for the system of equations of two-speed motion of two-phase media, J Appl Math Mech 46 (1) (1982) 66–74. doi:10.1016/0021-8928(82)90084-3.

[39] J. A. Trapp, The mean flow character of two-phase flow equations, Int J Multiphase Flow 12 (2) (1986) 263–276. doi:10.1016/0301-9322(86)90029-7.

[40] W. D. Fullmer, V. H. Ransom, M. A. Lopez de Bertodano, Linear and nonlinear analysis of an unstable, but well-posed, one-dimensional two-fluid model for two-phase flow based on the inviscid Kelvin–Helmholtz instability, Nucl Eng Des 268 (2014) 173–184. doi:10.1016/j.nucengdes.2013.04.043.

[41] G. S. Arnold, D. A. Drew, R. T. Lahey, An assessment of multiphase flow models using the second law of thermodynamics, Int J Multiphase Flow 16 (3) (1990) 481–494. doi:10.1016/0301-9322(90)90077-V.

[42] T. Vazquez-Gonzalez, Schémas numériques mimétiques et conservatifs pour la simulation d'écoulements multiphasiques compressibles, Ph.D. thesis, Université Paris–Saclay, France, 2016SACLC051 (2016).
URL https://www.theses.fr/2016SACLC051

[43] T. Vazquez-Gonzalez, A. Llor, C. Fochesato, A novel GEEC (Geometry, Energy, and Entropy Compatible) procedure applied to a staggered direct-ALE scheme for hydrodynamics, Eur J Mech B Fluids 65 (2017) 494–514. doi:10.1016/j.euromechflu.2017.05.003.

[44] R. W. Lyczkowski, The history of multiphase science and computational fluid dynamics; a personal memoir, Mech Engrg Ser, Springer, 2018. doi:10.1007/978-3-319-66502-3.

[45] Y. Tambour, A Lagrangian sectional approach for simulating droplet size distribution of vaporizing fuel sprays in a turbulent jet, Combust Flame 60 (1) (1985) 15–28. doi:10.1016/0010-2180(85)90115-4.

[46] J. B. Greenberg, I. Silverman, Y. Tambour, On the origins of spray sectional conservation equations, Combust Flame 93 (1–2) (1993) 90–96. doi:10.1016/0010-2180(93)90085-H.

[47] F. Laurent, M. Massot, Multi-fluid modelling of laminar polydisperse spray flames: origin, assumptions and comparison of sectional and sampling methods, Combust Theor Model 5 (4) (2001) 537–572. doi:10.1088/1364-7830/5/4/303.

[48] M. Massot, Eulerian multi-fluid models for polydisperse evaporating sprays, in: D. L. Marchisio, R. O. Fox (Eds.), Multiphase Reacting Flows: Modelling and Simulation, Vol. 492 of CISM International Centre for Mechanical Sciences, Springer, 2007, pp. 79–123. doi:10.1007/978-3-211-72464-4_3.

[49] J. G. Trulio, K. R. Trigger, Numerical solution of the one-dimensional Lagrangian hydrodynamic equations, Tech. Rep. UCRL-6267, Lawrence Radiation Laboratory (1961).
URL https://www.osti.gov/servlets/purl/4782302

[50] C. W. Hirt, A. A. Amsden, J. L. Cook, An arbitrary Lagrangian–Eulerian computing method for all flow speeds, J Comput Phys 14 (3) (1974) 227–253. doi:10.1016/0021-9991(74)90051-5.

[51] W. Boscheri, M. Dumbser, O. Zanotti, High order cell-centered Lagrangian-type finite volume schemes with time-accurate local time stepping on unstructured triangular meshes, J Comput Phys 291 (2015) 12–150. doi:10.1016/j.jcp.2015.02.052.

[52] J. Breil, T. Harribey, P.-H. Maire, M. Shashkov, A multi-material ReALE method with MOF interface reconstruction, Comput Fluids 83 (2013) 115–125. doi:10.1016/j.compfluid.2012.08.015.

[53] R. Loubere, P.-H. Maire, M. Shashkov, J. Breil, S. Galera, ReALE: a Reconnection-based Arbitrary-Lagrangian–Eulerian method, J Comput

Phys 229 (12) (2010) 4724–4761. doi:10.1016/j.jcp.2010.03.011.

[54] L. G. Margolin, Arbitrary Lagrangian–Eulerian (ALE) methods a personal perspective, Tech. Rep. Report LA-UR-13-24124, Los Alamos National Laboratory (2013).

[55] W. J. Rider, E. Love, M. K. Wong, O. E. Strack, S. V. Petney, D. A. Labreche, Adaptive methods for multi-materials ALE hydrodynamics, Internat J Numer Methods Fluids 65 (11–12) (2011) 1325–1337. doi:10.1002/fld.2365.

[56] D. Kah, Prise en compte des aspects polydispersés pour la modélisation d'un jet de carburant dans les moteurs à combustion interne, Ph.D. thesis, École Centrale Paris, France, 2010ECAP0044 (2010).
URL https://tel.archives-ouvertes.fr/tel-00618786v2/document

[57] D. Kah, O. Emre, Q. H. Tran, S. de Chaisemartin, S. Jay, F. Laurent, M. Massot, High order moment method for polydisperse evaporating sprays with mesh movement: application to internal combustion engines, Int J Multiphase Flow 71 (2015) 38–65. doi:10.1016/j.ijmultiphaseflow.2014.12.004.

[58] P.-H. Cournède, Un schéma bilagrange plus projection pour la simulation bifluide des instabilités de mélanges, Ph.D. thesis, École Centrale Paris, France, 2001ECAP0732, english version: http://cournede.digiplante.free.fr/Doc/thesis.ps (2001).
URL https://www.theses.fr/2001ECAP0732

[59] M. Kucharik, M. Shashkov, Conservative multi-material remap for staggered multi-material Arbitrary Lagrangian–Eulerian methods, J Comput Phys 258 (2014) 268–304. doi:10.1016/j.jcp.2013.10.050.

[60] A. H. Akselsen, O. J. Nydal, Applying multiple grids to a multi-field model – the resolution requirements of individual fields in the two-fluid model for 1D pipe flow, J Dispersion Sci Technol 36 (10) (2015) 1378–1387. doi:10.1080/01932691.2014.987783.

[61] A. H. Akselsen, A dual grid method for the compressible two-fluid model which combines robust flux splitting methodology with high-resolution capturing of incompressible dynamics, Chem Eng Sci 172 (2017) 707–721. doi:10.1016/j.ces.2017.07.013.

[62] J. von Neumann, R. D. Richtmyer, A method for the numerical calculation of hydrodynamic shocks, J Appl Phys 21 (3) (1950) 232–237. doi:10.1063/1.1699639.

[63] M. L. Wilkins, Calculation of elastic–plastic flow, in: B. Alder, S. Fernbach, M. Rotenberg (Eds.), Fundamental Methods in Hydrodynamics, Vol. 3 of Methods in Computational Physics: Advances in Research and Applications, Academic Press, 1964, pp. 211–262.

[64] A. Llor, A. Claisse, C. Fochesato, Energy preservation and entropy in Lagrangian space- and time-staggered hydrodynamic schemes, J Comput Phys 309 (2016) 324–349. doi:10.1016/j.jcp.2015.12.044.

[65] A. Marbœuf, Schémas ALE multi-matériaux totalement conservatifs pour l'hydrodynamique, Ph.D. thesis, Université Paris–Saclay, France, 2018SACLX015 (2018).
URL https://www.theses.fr/2018SACLX015

[66] U. M. Ascher, R. I. McLachlan, On symplectic and multisymplectic schemes for the KdV equation, J Sci Comput 25 (1–2) (2005) 83–104. doi:10.1007/s10915-004-4634-6.

[67] A. Llor, T. Vazquez-Gonzalez, Geometry, Energy, and Entropy Compatible (GEEC) variational approaches to various numerical schemes for fluid dynamics, in: F. Nielsen, F. Barbaresco (Eds.), Geometric Science of Information. GSI 2019, Vol. 11712 of Lecture Notes in Computer Science, Springer, 2019, pp. 559–567. doi:10.1007/978-3-030-26980-7_58.

[68] S. K. Godunov, A difference method for numerical calculation of discontinuous solutions of the equations of hydrodynamics, Mat Sb (NS) 47 (89) (3) (1959) 271–306.
URL https://mi.mathnet.ru/eng/msb4873

[69] J. M. Wendlandt, J. E. Marsden, Mechanical integrators derived from a discrete variational principle, Physica D 106 (3-4) (1997) 223–246. doi:10.1016/S0167-2789(97)00051-1.

[70] E. Tonti, Why starting from differential equations for computational physics?, J Comput Phys 257 (B) (2014) 1260–1290. doi:10.1016/j.jcp.2013.08.016.

[71] M. Gerritsma, An introduction to a compatible spectral discretization method, Mech Adv Mater Struct 19 (1–3) (2012) 48–67. doi:10.1080/15376494.2011.572237.

[72] Physics-compatible numerical methods, J Comput Phys 257 (B). doi:10.1016/j.jcp.2013.10.015.

[73] H. Goldstein, C. P. Poole, J. L. Safko, Classical mechanics, Addison–Wesley, 1950.
URL https://www.pearson.com/us/higher-education/program/Goldstein-Classical-Mechanics-3rd-Edition/PGM170105.html

[74] R. Prix, Variational description of multifluid hydrodynamics: uncharged fluids, Phys Rev D 69 (4) (2004) 043001. doi:10.1103/PhysRevD.69.043001.

[75] A. Bedford, D. S. Drumheller, A variational theory of immiscible mixtures, Arch Ration Mech Anal 68 (1978) 37–51. doi:10.1007/BF00276178.

[76] J. A. Geurst, Virtual mass in two-phase bubbly flow, Physica A 129 (2) (1985) 233–261. doi:10.1016/0378-4371(85)90168-2.

[77] J. A. Geurst, Two-fluid hydrodynamics of bubbly liquid/vapour mixture including phase change, Philips J Res 40 (1985) 352–374.
URL https://www.extra.research.philips.com/hera/people/aarts/_Philips%20Bound%20Archive/PJR/PJR-40-1985-352.pdf

[78] J. A. Geurst, Variational principles and two-fluid hydrodynamics of bubbly liquid/gas mixtures, Physica A 135 (2) (1986) 455–486. doi:10.1016/0378-4371(86)90154-8.

[79] M. B. Liu, G. R. Liu, Smoothed Particle Hydrodynamics (SPH): an overview and recent developments, Arch Computat Methods Eng 17 (1) (2010) 25–76. doi:10.1007/s11831-010-9040-7.

[80] M. S. Shadloo, G. Oger, D. Le Touzé, Smoothed particle hydrodynamics method for fluid flows, towards industrial applications: motivations, current state, and challenges, Comput Fluids 136 (2016) 11–34. doi:10.1016/j.compfluid.2016.05.029.

[81] E. P. Fahrenthold, J. C. Koo, Discrete Hamilton's equations for viscous compressible fluid dynamics, Comput Methods Appl Mech Eng 178 (1) (1999) 1–22. doi:10.1016/S0045-7825(99)00100-0.

[82] J. C. Koo, E. P. Fahrenthold, Discrete Hamilton's equations for Arbitrary Lagrangian–Eulerian dynamics of viscous compressible flow, Comput Methods Appl Mech Eng 189 (3) (2000) 875–900. doi:10.1016/S0045-7825(99)00405-3.

[83] E. P. Fahrenthold, C. R. Hean, Discrete Lagrange equations for thermofluid systems, J Dyn Syst Meas Contr 130 (1) (2008) 011009. doi:10.1115/1.2807084.

[84] C. R. Hean, Discrete Lagrange equations for reacting thermofluid systems, Ph.D. thesis, University of Texas at Austin, USA (2009).
URL https://repositories.lib.utexas.edu/handle/2152/18414

[85] C. R. Hean, E. P. Fahrenthold, Discrete Lagrange equations for reacting thermofluid dynamics in arbitrary Lagrangian–Eulerian frames, Comput Methods Appl Mech Eng 313 (2017) 303–320. doi:10.1016/j.cma.2016.10.001.

[86] M. Chhay, A. Hamdouni, Lie symmetry preservation by finite difference schemes for the Burgers equation, Symmetry 2 (2) (2010) 868–883. doi:10.3390/sym2020868.

[87] M. Desbrun, E. S. Gawlik, F. Gay-Balmaz, V. Zeitlin, Variational discretization for rotating stratified fluids, Discrete Continuous Dyn Syst 34 (2) (2013) 477–509. doi:10.3934/dcds.2014.34.477.

[88] D. Pavlov, P. Mullen, Y. Tong, E. Kanso, J. E. Marsden, M. Desbrun, Structure-preserving discretization of incompressible fluids, Physica D 240 (6) (2011) 443–458. doi:10.1016/j.physd.2010.10.012.

[89] W. Bauer, F. Gay-Balmaz, Towards a geometric variational discretization of compressible fluids: the rotating shallow water equations, ArXiv e-prints 1711 (2017) 10617.
URL https://arxiv.org/abs/1711.10617

[90] Z. Ge, J. E. Marsden, Lie–Poisson Hamilton–Jacobi theory and Lie–Poisson integrators, Phys Lett A 133 (3) (1988) 134–139. doi:10.1016/0375-9601(88)90773-6.

[91] J. W. Strutt (Lord Rayleigh), Some general theorems relating to vibrations, Proc London Math Soc s1–4 (1) (1871) 357–368. doi:10.1112/plms/s1-4.1.357.

[92] J. Serrin, Mathematical principles of classical fluid mechanics, in: S. Flügge, C. Truesdell (Eds.), Fluid Dynamics I, Vol. VIII/1 of Encyclopedia of Physics, Springer, 1959, pp. 125–263. doi:10.1007/978-3-642-45914-6_2.

[93] C. C. Lin, Hydrodynamics of Helium II, in: G. Careri (Ed.), Proceedings of the International School of Physics "Enrico Fermi," Course XXI, Liquid Helium, Academic Press, 1963, pp. 93–146.

[94] R. L. Seliger, G. B. Whitman, Variational principles in continuum mechanics, Proc R Soc London, Ser A 305 (1480) (1968) 1–25. doi:10.1098/rspa.1968.0103.

[95] J. W. Herivel, The derivation of the equations of motion of an ideal flow by Hamilton's principle, Math Proc Cambridge Philos Soc 51 (2) (1955) 344–349. doi:10.1017/S0305004100030267.

[96] F. P. Bretherton, A note on Hamilton's principle for perfect fluids, J Fluid Mech 44 (1) (1970) 19–31. doi:10.1017/S0022112070001660.

[97] S. Gavrilyuk, R. Saurel, Mathematical and numerical modeling of two-phase compressible flows with micro-inertia, J Comput Phys 175 (1) (2002) 326–360. doi:10.1006/jcph.2001.6951.

[98] J.-M. Ghidaglia, personnal communication (2000).

[99] S. T. Munkejord, S. Evje, T. Flåtten, A MUSTA scheme for a nonconservative two-fluid model, SIAM J Sci Comput 31 (4) (2009) 2587–2622. doi:doi.org/10.1137/080719273.

[100] J. J. Kreeft, B. Koren, A new formulation of Kapila's five-equation model for compressible two-fluid flow, and its numerical treatment, J Comput Phys 229 (18) (2010) 6220–6242. doi:10.1016/j.jcp.2010.04.025.

[101] A. E. Mattsson, W. J. Rider, Artificial viscosity: back to the basics, Int J Numer Meth Fluids 77 (7) (2015) 400–417. doi:10.1002/fld.3981.

[102] L. G. Margolin, The reality of artificial viscosity, Shock Waves 29 (1) (2019) 27–35. doi:10.1007/s00193-018-0810-8.

[103] W. D. Fullmer, S. Y. Lee, M. A. Lopez de Bertodano, An artificial viscosity for the ill-posed one-dimensional incompressible two-fluid model, Nucl Technol 185 (3) (2014) 1–13. doi:10.13182/NT13-66.

[104] Y. B. Zel'dovich, Y. P. Raizer, Physics of shock waves and high-temperature hydrodynamic phenomena, Academic Press, 1967.

[105] W. F. Noh, Errors for calculations of strong shocks using an artificial viscosity and an artificial heat flux, J Comput Phys 72 (1) (1987) 78–120. doi:10.1016/0021-9991(87)90074-X.

[106] R. DeBar, Fundamentals of the Kraken code, Tech. Rep. Report UCIR-17366, Lawrence Livermore National Laboratory (1974). doi:10.2172/7227630.

[107] C. Paulin, E. Heulhard de Montigny, A. Llor, Towards isotropic transport with co-meshes, Coupled Syst Mech 9 (1) (2020) 63–75. doi:10.12989/csm.2020.9.1.063.

[108] J.-M. Ghidaglia, A. Kumbaro, G. Le Coq, On the numerical solution to two fluid models via a cell centered finite volume method, Eur J Mech B Fluids 20 (6) (2001) 841–867. doi:10.1016/S0997-7546(01)01150-5.

[109] S. Dellacherie, Analysis of Godunov type schemes applied to the compressible Euler system at low Mach number, J Comput Phys 229 (4) (2010) 978–1016. doi:10.1016/j.jcp.2009.09.044.

[110] S. Shanmuganathan, D. L. Youngs, J. Griffond, B. Thornber, R. J. R. Williams, Accuracy of high-order density-based compressible methods in low Mach vortical flows, Int J Numer Meth Fluids 74 (5) (2014) 335–358. doi:10.1002/fld.3853.

[111] M. Sun, An implicit cell-centered Lagrange–Remap scheme for all speed flows, Comput Fluids 96 (2014) 397–405. doi:10.1016/j.compfluid.2013.07.019.

[112] C. Chalons, M. Girardin, S. Kokh, An all-regime Lagrange–Projection like scheme for the gas dynamics equations on unstructured meshes, Commun Comput Phys 20 (1) (2016) 188–233. doi:10.4208/cicp.260614.061115a.

[113] E. Tadmor, Entropy stability theory for difference approximations of nonlinear conservation laws and related time-dependent problems, Acta Numer 12 (2003) 451–512. doi:10.1017/S0962492902000156.

[114] B. Després, F. Lagoutière, Numerical resolution of a two-component compressible fluid model with interfaces, Prog Comput Fluid Dyn 7 (6) (2007) 295–310. doi:10.1504/PCFD.2007.014680.

[115] R. Menikoff, B. J. Plohr, The Riemann problem for fluid flow of real materials, Rev Mod Phys 61 (1) (1989) 75–130. doi:10.1103/RevModPhys.61.75.

[116] G. A. Sod, A survey of several finite difference methods for systems of nonlinear hyperbolic conservation laws, J Comput Phys 27 (1) (1978) 1–31. doi:10.1016/0021-9991(78)90023-2.

[117] V. H. Ransom, Numerical benchmark test No 2.1: faucet flow, Multiphase Sci Technol 3 (1-4) (1987) 465–467. doi:10.1615/MultScienTechn.v3.i1-4.280.

[118] P. J. O'Rourke, D. M. Snider, An improved collision damping time for MP-PIC calculations of dense particle flows with applications to polydisperse sedimenting beds and colliding particle jets, Chem Eng Sci 65 (22) (2010) 6014–6028. doi:10.1016/j.ces.2010.08.032.

[119] P. Roe, Chapter 3 - Multidimensional upwinding, in: R. Abgrall, C. W. Shu (Eds.), Handbook of Numerical Methods for Hyperbolic Problems, Vol. 18 of Handbook of Numerical Analysis, Elsevier, 2017, pp. 53–80. doi:10.1016/bs.hna.2016.10.009.

[120] J. H. Stuhmiller, The influence of interfacial pressure forces on the character of two-phase flow model equations, Int J Multiphase Flow 3 (6) (1977) 551–560. doi:10.1016/0301-9322(77)90029-5.

[121] D. Bestion, The physical closure laws in the Cathare code, Nucl Eng Des 124 (3) (1990) 229–245. doi:10.1016/0029-5493(90)90294-8.

[122] D. Lhuillier, Phenomenology of inertia effects in a dispersed solid-fluid mixture, Int J Multiphase Flow 11 (4) (1985) 427–444. doi:10.1016/0301-9322(85)90068-0.

[123] J. A. Wallis, Dobson, The onset of slugging in horizontal stratified air-water flow, Int J Multiphase Flow 1 (1) (1973) 173–193. doi:10.1016/0301-9322(73)90010-4.

[124] D. L. Youngs, Modelling turbulent mixing by Rayleigh–Taylor instability, Physica D 37 (1–3) (1989) 270–287. doi:10.1016/0167-2789(89)90135-8.

Answer to Reviewers

Reviewer 1

The paper presents a multi-fluid numerical scheme for solving the backbone equations over a moving grid. The concept "Geometry, Energy, and Entropy Compatible" is discussed and the derivation of the coupled increment equations for fluids have been presented. Three 2D numerical test cases - including Sod's shock tube, Ransom's faucet, and a nine-fluids crossing test are presented. Unfortunately, I don't think the current manuscript reaches the standard for publication in IJMF and regret to recommend its rejection. The manuscript is more suitable for other numerical methods focused journals. – Various key ingredients involved in building the numerical scheme are very uncommon and closely related to multiphase physics: mimicking of the backbone non-dissipative but elliptic equations, least action principle, explicit multi-fluid Gibb's relationship, etc. Yet, a previous submission to a journal of numerical methods was rejected on the grounds that "this is merely physics." We actually pride ourselves of having built a scheme that is deeply grounded on basic physical principles. We thus believe that IJMF is the appropriate medium for this work where many readers will find answers to recurring questions regarding thermodynamic consistency of multi-fluid schemes. – The following is a list of issues motivating my recommendation for rejection.

1. There are many 3D numerical studies for multiphase flows and multi-physics based on ALE. However, it is only 2D study here. – As now explicitly commented in new Section 1.5, numerical schemes can be found which meet *some* but, to our knowledge, not *all* of our specifications in Section 1.4. We would happily analyze and cite any accessible reference to a scheme complying with all the specifications. As of 3D studies, they would only marginally illustrate the scheme capabilities, would not affect any of its underlying principles, would require a significant investment in code and computer technicalities, would significantly lengthen the manuscript (already 25 journal pages), and would reduce its legibility and consistency. –
2. The numerical examples here are all classical benchmark problems and there is no convergence study here. – As now explicitly commented in new Section 1.5, the numerical schemes are only "superficially classic" and, because of the ellipticity issues, convergence studies are deliberately set aside for later works involving dissipation terms. – In addition, there are no comparisons with other numerical methods to see its advantage or efficiency. – Here again, we would need to have another scheme with similar capabilities in order to make comparisons. It must be stressed that the aim of this work is not to provide a somewhat novel "better-than" scheme for a somewhat standard situation, but rather to provide one that "does it" in strenuous cases. The numerical tests mostly support this capability. –
3. Most parts of the manuscripts focus on the derivation of the numerical scheme with some simple benchmark cases, which might be more suitable for a numerical method journal. – See first comment above. –
4. Artificial viscosity has been introduced in the numerical treatment. What happens for the shock profiles if there is no artificial viscosity? – This point has been investigated since artificial viscosity was first introduced [for a review, see for instance 101]: shocks generate large oscillations, become unstable, and eventually crash the calculations. –
5. The numerical results are only shown for the density and volume fraction. What about the internal energy and pressure? – In order to avoid excessive lengthening of the manuscript, the usual choice of only showing density and volume fraction was done. Internal energy and pressure are less directly interpreted and would bring marginal supplementary understanding. – The conservation property of the results has not been discussed in the result section, especially for the mass in the multi-fluid systems. – As now explicitly commented in new Section 1.5, the *exact* conservation properties are established from the rigorous formal derivation. It comes from the inherent conservation to round off errors of all finite volume approches. –

Reviewer 2

This manuscript addresses an interesting topic in the field of multi-fluid flow problems. They developed a compressible multi-fluid backbone model with arbitrary Lagrangian-Eulerian descriptions for the simulations. Second-order accuracy in temporal and spatial discretizations in a Lagrangian limit is satisfied. Some advantages could be found in this model; for instance, the arbitrary number of fluids, stabilization for shock capture and the stable numerical treatment with high CFL conditions. It is good to see an applicable computational work in this area of research after testifying three two-dimensional cases, including the Sod's shock tube variant, Ransom's faucet variant and supersonic nine-fluid crossing test on a shrink-then-stretch swirling grid. The numerical results performed in this manuscript are authentic and meaningful. The manuscript is also well-written and well-organized with clear content. I believe that this is a competent work, with novel results and can be interest to the readers. In my viewpoint, it could be acceptable for publication in the International Journal for Multiphase Flow. – We are grateful to the Reviewer for his appreciation. – However, two issues in simulations need to be clarified in this manuscript for improving the information, as follows

1. It is necessary to add the convergence test in each testing case. – As now explicitly commented in new Section 1.5 and because of the ellipticity issues, convergence studies are deliberately set aside for later works involving dissipation terms. Numerical tests have been chosen to illustrate the proof-of-concept and the gains brought by the scheme. They are not meant to be an extensive test for the time being. –
2. The criterion and limitation in wide use should be elaborated. – A sentence was added to Section 4.8 to specify length scale for artificial viscosity. The notations for characteristic lengths have also been changed and made consistent. –